Separation and Purification Technology 323 (2023) 124387

Contents lists available at ScienceDirect

Separation and Purification Technology

journal homepage: www.elsevier.com/locate/seppur

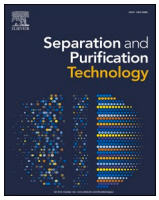

Amphiphilic block copolymers as dual flocculation-flotation agents for rapid solid–liquid separation of radioactive wastes

Alexander P.G. Lockwood [a,b,*], Georgina Wadsley [a], Nicholas J. Warren [a], Jeffrey Peakall [c], Grant B. Webber [d], Erica J. Wanless [d], Dominic Rhodes [b], Martyn Barnes [b], David Harbottle [a], Timothy N. Hunter [a]

[a] School of Chemical and Process Engineering, University of Leeds, Leeds LS2 9JT, United Kingdom
[b] Particles with Fluids Centre of Expertise, Sellafield Ltd, Birchwood, Warrington WA3 6GR, United Kingdom
[c] School of Earth and Environment, University of Leeds, Leeds LS2 9JT, United Kingdom
[d] ARC Centre of Excellence for Enabling Eco-Efficient Beneficiation of Minerals, University of Newcastle, Callaghan, NSW 2308, Australia

ARTICLE INFO

Keywords:
Flotation
Flocculation
Amphiphilic block copolymer
Polymeric collectors
Polymeric micelles
Magnesium hydroxide

ABSTRACT

The potential of poly(acrylic acid)-*b*-poly(*n*-butyl acrylate) as a dual flocculant-collector in combined flotation-sedimentation dewatering operations was investigated. The amphiphilic block copolymers were synthesised with consistent hydrophilic chain lengths and varying hydrophobic chain lengths. Various techniques were employed to analyse polymer behaviour at the air–water interface, being interfacial surface tension and dilational visco-elasticity. Polymer adsorption onto $Mg(OH)_2$ was determined differentially using UV–Vis spectroscopy. Floc structures were determined using static light scattering, and flocculation-flotation performance was analysed using settling tests and flotation cell material balances. Results showed that longer hydrophobic chains were less surface-active, reducing foamability and water entrainment. The unimer-micellar adsorption transition points were identified through viscoelastic properties and particle adsorption studies. A distinct change in floc density and structure was observed for the largest molecular weight copolymer when the dosed concentration increased into the micellar adsorption region, suggesting a pseudo-bridging flocculation mechanism. Settling rates were significantly higher for particles flocculated with the larger molecular weight polymer, correlating to their larger aggregate sizes, especially over the micellar transition point. The largest molecular weight block copolymer demonstrated superior collection efficiency compared to the traditional surfactant, sodium dodecylsulfate (SDS), below its micellar adsorption transition point. However, beyond this point, the lack of exposed hydrophobic blocks hindered the hydrophobisation of $Mg(OH)_2$ particles, reducing collection efficiency. Comparing flotation cell particle size distributions, it was suggested that recovery may be hydrodynamically hindered by the largest floc sizes, though recovery was observed for particles in the order of < 600 μm.

1. Introduction

Flotation has demonstrated its effectiveness as a mineral separation technique and also as a promising technology for rapid solid–liquid separation in water treatment processes [1–6]. Flotation cells offer the advantage of being easily retrofitted to existing facilities and are simple to maintain. Additionally, their wide operational envelope allows for greater confidence in accepting varying feed compositions [7]. However, whilst there is a chemical robustness, flotation suffers from a limited hydrodynamic operational envelope [8,9]. Particles below the lower limit of acceptance (fines of $<$ 50–100 μm) may be too small and lack sufficient inertia to overcome slip streams generated from rising bubbles in the flotation cell, preventing bubble attachment [10,11]. Particles above the upper limit of acceptance (coarse particles), are too heavy for bubble buoyancy to facilitate adequate mass transfer to the upper foam phase. Poor coarse particle selection has been attributed to low particle-bubble detachment contact angles contrary to effective flotation, which is facilitated by the tenacity of bubble attachment (capillary, hydrostatic pressure forces and buoyancy of the particle volume submerged in the liquid). Additionally, inertial/gravitational forces alter the radial slip velocity across the bubble surface, resulting in relatively high detachment energy [10,12].

* Corresponding author.
E-mail address: a.p.g.lockwood@leeds.ac.uk (A.P.G. Lockwood).

https://doi.org/10.1016/j.seppur.2023.124387
Received 12 May 2023; Received in revised form 18 June 2023; Accepted 18 June 2023
Available online 22 June 2023

Whilst surfactants are regularly used as collectors in industry due to their surface-active amphiphilic nature [4,13–16], they have been found to be poor particle aggregators [3,17,18]. Additionally, surfactants have been associated with greater water loss in flotation processes from the high-water content of foams generated, leading to poor dewatering ratios and low collection efficiency [19–24]. Alternatively, polymeric flocculants have proven to be highly effective at affecting particle size distributions (PSDs) to produce larger aggregates [25–37], potentially decreasing the level of fines in flotation operations. However, the diameters of particles across the distribution will also increase, meaning a larger proportion will exist above the operational envelope for successful flotation [38]. Combining flocculation-flotation with subsequent gravity driven sedimentation may successfully remove these non-floatable coarse aggregates, where selectivity is not required in industries such as water treatment and nuclear decommissioning [39,40,3]. Traditional large molecular weight charged polyelectrolytes used for flocculation and sedimentation cannot be used as flotation collectors, since they cannot impart hydrophobicity to particle surfaces as effectively as surfactants. This limitation necessitates the use of additional collector agents that compete for adsorption with the polymers, or the design of alternative polymer collectors.

To address the behavioural modification required for both flocculation and hydrophobisation of particles, the use of temperature responsive and novel collector polymers has received a large amount of attention in recent years [38,39,42–49]. These macromolecules function as dual flocculation-collector agents displaying several advantages, including the ability to flocculate particles and use a 'thermal switch' to control bed sedimentation density [42,43,46,47]. However, this thermal transition functionality is also a caveat to technological viability. Heating suspensions on industrial scales is highly energy intensive. Interest in developing collectors for mineral processing has increased in line with industry focus on 'smart processing', which aims to reduce energy requirements and water consumption. Collectors that can produce high particle load, low water content foams without the need for heating are of particular interest.

An alternative to temperature responsive polymers are amphiphilic block copolymers. Like traditional surfactants, amphiphilic block copolymers undergo self-assembly to form nanostructures with morphological features that are dependent on the relative length of their hydrophobic and hydrophilic blocks [50]. They can also adsorb onto solid substrates either as individual copolymer chains, forming a brush-like layer; or by micellar adsorption depending on dosed concentration rather than stimuli triggers [51–56]. This mechanism of hydrophobisation by adsorption in the monolayer concentration regime is analogous to traditional surfactants when used as collectors [57]. A further advantage is that higher molecular weight hydrophobic blocks have little effect on surface tension, with critical micelle concentrations (CMCs) decreasing with increasing hydrophobic blocks, allowing control over water loss [58–62]. In the case of ionic species, the hydrophilic block will have a high affinity to oppositely charged particle surfaces in suspensions, adopting a tight patch-wise adsorption mechanism and facilitating charge patch flocculation below the copolymer CMC [34,37,45]. Above the CMC, micellar adsorption has been shown to produce a pseudo-bridging flocculation mechanism through micelle formation with entanglement of the exposed hydrophobic tails on the particle surface, producing dense hydrophobic layers which have been reported to liberate water as they rearrange to reduce free energy [45,63]. Effectively, the micellisation formation mechanism allows copolymers to act as moderate flocculation agents and excellent hydrophobic surface modifiers as unimers below their CMC, and above the CMC, facilitate larger structures associated with excellent polymeric settling aids [34,64,65].

Herein, a series of amphiphilic poly(acrylic acid)-*b*-poly(*n*-butyl acrylate) (PAA-PnBA) diblock copolymers were synthesised by reversible addition − fragmentation chain-transfer (RAFT) mediated emulsion polymerisation [66]. During this process, a hydrophilic PAA block of fixed length was extended with varying lengths of hydrophobic PnBA, to act as dual dewatering agents. Characterisation of the interfacial behaviour of the polymers in solution and on particle surfaces was also performed. Air-water surface tension and dilational viscoelasticity were measured to probe the mechanical strength and resistance to bubble coalescence of generated foams, which has been linked to flotation performance [67–69]. Copolymer adsorption on waste particle surfaces was also investigated to determine the transition from unimer to micellar adsorption, which may possess differing flocculation properties [45]. Here, suspensions of fine magnesium hydroxide ($Mg(OH)_2$) were used, owing to their cationic surface charge, allowing electrostatic attraction to the charged PAA blocks. Additionally, $Mg(OH)_2$ is a common nuclear waste analogue, as it is a corrosion product from long term underwater storage of Magnox alloy used in UK nuclear fuel cladding [70]. $Mg(OH)_2$ has also used in previous investigations, where its sedimentation with traditional polyelectrolytes and flotation with surfactant collectors have been determined [26,57]. Likewise, here, the block copolymers were investigated for their performance as both sedimentation and flotation aids in a batch flotation cell, using methyl isobutyl carbinol frothing agent. Performance was assessed by measuring particle and water mass recoveries, comparing dewatering efficiencies with a collection efficiency factor.

2. Materials and experimental methodology

2.1. Materials

Fine magnesium hydroxide, $Mg(OH)_2$, powder (Versamag, Martin Marietta, US) was used for flocculation and flotation experiments, as in previous work by the current authors [26,57]. $Mg(OH)_2$ is made up of aggregates of pseudo-hexagonal platelets similar to those reported by Johnson et al. [71] and Maher et al. [72]. Surface charge analysis found the zeta-potential to be ~+12 mV indicating a cationic surface, a specific surface area of ~ 8 $m^2 \cdot g^{-1}$ was measured using BET analysis as described in the authors' previous work [26]. $Mg(OH)_2$ was also found to be self-buffering when suspended in water, due to its semi-soluble nature, maintaining a suspension pH of ~ 10.10 with an initial solids concentration of 2.5 vol%. It should also be noted that in previous work, $Mg(OH)_2$ was found to aggregate to a degree overtime [57].

For the polymeric synthesis of the PAA-*b*-PnBA amphiphilic block copolymers (referred to from hereon as block copolymers), the monomers acrylic acid (AA; Acros Organics 99.5% extra pure stabilised) and *n*-butyl acrylate (nBA: VWR > 98%, stabilised with up to 50 ppm 4-methoxyphenol) were selected to form the hydrophilic and hydrophobic segments respectively. The AA and nBA monomers were polymerised in the presence of 3-((((1-carboxylethyl)thio)carbonothioly)thio)propanoic acid (CCTP; Boron Molecular) which acted as a RAFT chain transfer agent [54,73,74]. The polymerisation was initiated using 4,4′-azobis(4-cyanovaleric acid) (ACVA; Merck ≥ 75%). Methanol (Sigma-Aldrich ≥ 99.6%) was used as a compatible diluent for AA and nBA, allowing characterisation before the emulsion polymerisation stage, as nBA is not soluble in water and prevents NMR spectroscopy of the reagents prior to polymerisation. For NMR spectroscopy analysis, 3-(trimethylsilyl)-1-propanesulfonic acid sodium salt (TMS salt; Sigma Aldrich; 99%) was used as an internal standard to enable calculation of nBA conversion.

For the flotation and interface modification investigations, sodium dodecylsulfate (SDS) (TOKU-E, USA ≥ 99%) was used as a comparative surfactant collector, at a concentration of 16400 μM (where the critical micelle concentration of SDS in water is ~ 8200 μM [75]). For all flotation experiments, 4-methyl-2-pentanol (MIBC) (Sigma-Aldrich, 98%) was used as a frothing agent.

2.2. Synthesis and characterisation of poly(acrylic acid)-b-poly(n-butyl acrylate)

A detailed description of polymer synthesis is given within the Electronic Supplementary Materials (ESM, Section S1). First, a PAA macromolecular chain transfer agent (macro-CTA) was prepared by aqueous RAFT solution polymerisation of AA (see Fig. 1A), which was subsequently chain-extended with a *n*-butyl acrylate (nBA) chain via aqueous RAFT emulsion polymerisation. The latter process has recently been well reported and is beneficial in enabling aqueous polymerisation of insoluble monomers [73]. An array of three target block copolymers were selected for this work. Firstly, PAA was synthesised using AVCA as a thermal initiator and CCTP as the chain-transfer-agent (reaction A in Fig. 1). A target degree of polymerisation (*Dp*) of 160 was chosen for the macro-CTA, which represents a relative $MW = \sim 1.15 \times 10^4$ g·mol^{-1}. This is a comparable order of magnitude to polymeric flocculants which utilise a 'charge patch' flocculation mechanism to successfully aggregate particles into tight compact flocs [76]. A solids concentration of 30 wt% was selected for a relatively low aqueous macro-CTA solution viscosity for ease of manipulation.

Aliquots of the PAA macro-CTA polymer solution were extracted and analysed using a Magritek® (Germany) ^{1}H Spinsolve 60 MHz benchtop NMR spectrometer, determining the achieved macro-CTA *Dp*. A conversion of 96% was achieved (estimated using the reduction in vinyl proton environment peaks, see ESM Fig. S1) giving a degree of polymerisation of 153. The reaction was quenched by introducing oxygen to the system to ensure high retention of terminal RAFT trithiocarbonate groups, required for effective chain extension (See Fig. 1B). The PAA was then used as a macro-CTA for the RAFT emulsion polymerisation stage (reaction B in Fig. 1). The polymerisation process was repeated using the macro-CTA *in lieu* of CCTP with the nBA monomer, with targeted PnBA *Dp* of 25, 100 and 200 to give three separate polymers for investigation (for reagent ratio details, please see ESM Table S1). The RAFT polymerisation reaction was carried out until completion and NMR spectroscopy indicated monomer conversions of > 99% (judged by near complete disappearance of the signals relating to the vinyl protons in the NMR spectrum, see ESM Fig. S2). The solids concentration for the block copolymers was also 30 wt% for ease of manipulation. During the polymerisation, successful chain formation was confirmed by an increase in turbidity of the samples, due to *in situ* self-assembly of the polymers to form polymer micelles. The three polymers, listed herein as PAA_{153}-*b*-$PnBA_{25}$, PAA_{153}-*b*-$PnBA_{100}$ and PAA_{153}-*b*-$PnBA_{200}$, were then each diluted in Milli-Q^{TM} water to make three stock solutions of 10000 ppm, which could be sampled and diluted as required for the experiments in this work. Unfortunately, the resulting polymers were insoluble in all available solvents used for gel permeation chromatography, meaning a measured molecular weight distribution could not be obtained. It is assumed that the total polymer *MW* (MW_p) is the sum of the products of the segment target molecular weight, MW_i, and corresponding conversion fraction for each segment, X_i (i.e. $MW_p = \sum_{i=1}^{n} MW_i \bullet X_i$). This is important for mass to molar conversions in order to compare on a molecular basis with the benchmarked surfactant system.

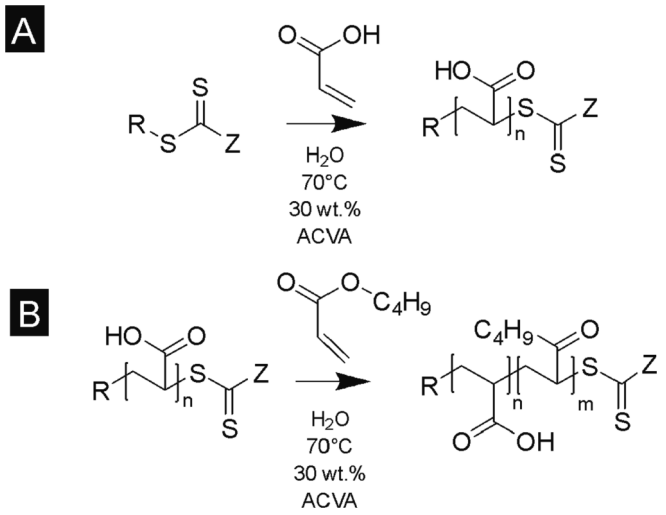

Fig. 1. Reaction scheme for the two-step synthesis of the block copolymer via aqueous RAFT solution polymerisation. A) Synthesis of the poly(acrylic acid)$_{152}$ macro chain transfer agent via aqueous solution RAFT. B) Chain extension with *n*-butyl acrylate via RAFT aqueous emulsion polymerisation reactions were carried out in an inert N_2 atmosphere at 70 °C with ACVA initiator and CCTP chain transfer agent.

2.3. Interfacial tension and viscoelasticity characterisation

The interfacial surface tension and dilational viscoelasticity were determined using a PAT-1 tensiometer (SINTERFACE Technologies, Germany) instrument. Utilising image analysis of a pendant drop to determine the principal radii of curvature of the drop, the Young-Laplace equation was used to calculate the dynamic interfacial surface tension [77]. The effect of polymer concentration on the surface tension and dilational viscoelasticity of aqueous polymer-water solutions was examined over the concentration range of 0–207 μM and 0–81 μM for PAA_{153}-*b*-$PnBA_{25}$ and PAA_{153}-*b*-$PnBA_{200}$ respectively. Polymers were prepared on a mass basis before conversion to molar for benchmark comparison explaining the molar ranges. SDS solutions (0–820 μM) were also measured for comparison to the polymers, and for comparison to previous work from the current authors using SDS as collector agents [57]. An oscillation period of 5 s and 10 complete cycles, with a pendant drop volume oscillation envelope of 9–11 μL, were selected based on previous investigations of surface tension and dilational viscoelasticity with the same instrument [78–80].

2.4. Polymer-particle adsorption

Adsorption experiments were performed for both PAA_{153}-*b*-$PnBA_{25}$ and PAA_{153}-*b*-$PnBA_{200}$ polymers, to represent the envelope of the hydrophobic block chain lengths investigated in this work, across a range of concentrations of 10–655 μM and 3–270 μM respectively. For each adsorption experiment, $Mg(OH)_2$ powder and polymer solution were placed in a centrifuge tube (15 mL) with a total volume of 10 mL, at a solid:liquid ratio of 1:100. The centrifuge tubes were placed in an ultrasonic bath (Clifton Sonic) for 20 min to ensure the breakup of any preformed $Mg(OH)_2$ aggregates. The samples were then put on a carousel stirrer at 40 rpm for 24 hrs for adsorption to occur. The suspensions were separated in a Megafuge 16R (Thermo Fisher Scientific, UK) at 8000 rpm for 30 min and the supernatant polymer solution was removed into a separate sample vial using a pipette. UV–visible spectroscopy was used to analyse supernatant polymer concentrations, as the carbonyl group on both PAA and PnBA is known to be a chromophore [81]. Solutions were analysed using a Cary 60 UV–VIS spectrometer (Agilent Technologies, UK).

The adsorption of block copolymers onto the $Mg(OH)_2$ was then characterised using the Freundlich isotherm, as previously undertaken for surfactant adsorption onto the same particles [57]. The linear Freundlich adsorption isotherm is shown in Eqn. (1), where q_e is the adsorption density of the polymers onto the $Mg(OH)_2$ surface (q_e is given in units of μmol·m^{-2} by dividing the solids concentration of $Mg(OH)_2$ by its specific surface area, $A_s = 8$ m^2·g^{-1}). C_e is the equilibrium concentration of polymer in the supernatant, *1/n* is a Freundlich constant (related to the adsorption intensity) and k_f is the Freundlich constant related to the adsorption capacity (μmol·m^{-2}).

$$Log(q_e) = Log(k_f) + \frac{1}{n} Log(C_e) \quad (1)$$

2.5. Floc structure characterisation

Floc structure characterisation was completed using a similar procedure to that of previous work by the current authors [26]. Static light scattering (SLS) was used to measure the fractal dimensions of the flocculated suspensions. Here, 20 mL suspensions were prepared using 2.5 vol% $Mg(OH)_2$ in Milli-Q^{TM} water and then sonicated for 20 min to breakup any preformed aggregates. Various concentrations of the block copolymers, PAA_{153}-*b*-$PnBA_{25}$ and PAA_{153}-*b*-$PnBA_{200}$, were then added and suspensions agitated using a magnetic stirrer for 20 min. The suspensions were then added to a Mastersizer 2000E (Malvern Panalytical Ltd) using a Hydro 2000SM aqueous dispersion cell. The unit was sheared at 900 rpm to ensure consistent flow of suspensions through the vertical optical window at concentrations within the instrument obscuration envelope. The obtained scattering intensity, *I(Q)*, and the scattering wave factor, *Q*, were then used to determine the fractal dimension of the flocs, denoted as d_f. As the relationship between the scattering intensity and scattering wave vector is established by the proportionality $I(Q) \propto Q^{-d_f}$ [82], the fractal dimension of the block copolymer-$Mg(OH)_2$ flocs can be determined by plotting *logI(Q)* with respect to *logQ* [82].

Visual microscopy was used to confirm the size and morphology of aggregates produced from suspensions dosed with polymers. Two samples were set up at different initial concentrations for each block copolymer (PAA_{153}-*b*-$PnBA_{25}$ at 207 μM and 345 μM, and PAA_{153}-*b*-$PnBA_{200}$ at 41 μM and 81 μM). A Morphologi G3 (Malvern Panalytical Ltd.) automated single element microscope measured floc samples on a floc by floc basis taken after 5 min of agitation in the flotation cell. A 4-slide plate was selected for dispersing the floc suspensions, where a droplet of the sample was added to each slide, sealing with a cover slip. The microscope setting was optimised, starting from the smallest magnification, taking images of each sample. A magnification of × 20 was selected for PAA_{153}-*b*-$PnBA_{25}$ and × 5 for PAA_{153}-*b*-$PnBA_{200}$. A differential z-stacking of 2 was selected to cover an appropriate depth of scanning, and the full scan area was selected to maximise sample size. Data were analysed and computed as a cumulative frequency distribution for comparison of floc population sizes. Floc sizes were compared between pre-flotation directly from the flotation cell and post-flotation from the collector tray (see Section 2.6) to establish the flotation separation floc size envelope and inform on post-flotation sedimentation.

2.6. Sedimentation and flotation performance and analysis

Visual observation of suspension-supernatant boundary level change with time was used to measure the influence of block copolymer concentration on hindered settling rates. Here, 12.31 g of $Mg(OH)_2$ was added to a measuring cylinder and dosed with 98 μM of MIBC, along with the required dose of block copolymer (for final solution concentrations of 35–245 μM and 14–81 μM for PAA_{153}-*b*-$PnBA_{25}$ and PAA_{153}-*b*-$PnBA_{200}$ respectively) and then made up to 210 mL with Milli-Q^{TM} water. The mixed flocculated suspensions were then transferred to 250 mL measuring cylinders, where the cylinders were inverted 5 times to evenly re-suspend flocs and the interfacial velocity was determined.

Flotation performance was investigated with 2.5 vol% $Mg(OH)_2$ suspensions that were prepared and pre-mixed by agitation in a bespoke flotation cell at 250 rpm with variable concentrations (35–245 μM and 14–81 μM for PAA_{153}-*b*-$PnBA_{25}$ and PAA_{153}-*b*-$PnBA_{200}$ respectively) of two block copolymers. Airflow into the bottom of the cell was set at 0.1 L min^{-1} and the agitator speed was reduced to 100 rpm to suspend larger particulates, but, minimise turbulence in the cell and prevent froth destabilisation. Foam generated above the air–water interface poured through the outlet at the top of the vessel and into a pre-weighed aluminium collection container. This container was weighed and placed into an oven for 24 hr to evaporate the water component of the foam, leaving behind the recovered particulates. The container was then weighed again to determine the performance indicators including mass percentage recovery, water recovery and the residual volume concentration in the cell (see ESM Section S2 and Eqns. S1-S3 respectively). The performance of the collectors was compared using a collector efficiency factor, ξ, shown in Eqn. (2), which is a ratio of the percentage of the particles to fluid recovered from the flotation cell. Here, $\xi > 1$ indicates there are more $Mg(OH)_2$ particles recovered than water by mass, where $\xi = 1$ there is equal particle–fluid extraction (entrainment) and when $\xi < 1$ there is more fluid being extracted than $Mg(OH)_2$ particles. The collection efficiency factor was then used to determine the optimum dose of collector to maximise solid–liquid separation.

$$\xi = \frac{P_{\%}}{100 - W_{\%}} \tag{2}$$

3. Results and discussion

3.1. Interfacial tension and dilational viscoelasticity

To compare the surface activity of the block copolymers with standard surfactants, Fig. 2A shows the change in interfacial surface tension (γ) as a function of dosed polymer concentration. The results are compared to SDS over a similar concentration range. PAA_{153}-*b*-$PnBA_{25}$, which has a shorter hydrophobic block, exhibits significantly higher surface activity than PAA_{153}-*b*-$PnBA_{200}$. It is also more surface active than SDS at equivalent concentrations, due to its much greater molecular weight, noting the maximum concentration of any solutions reported in Fig. 2A is only 10% of the reported CMC of SDS of 8.2 mM,

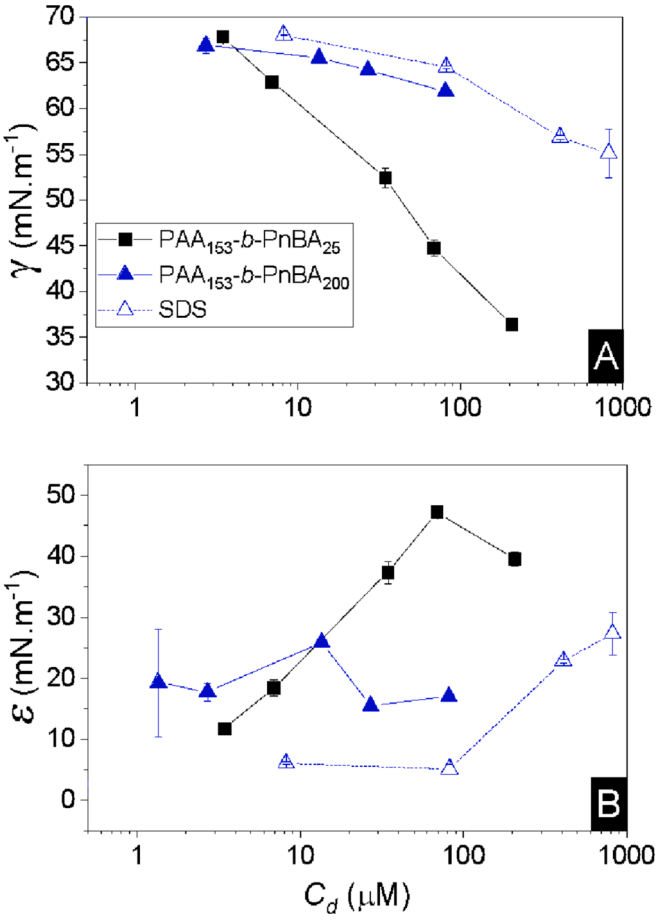

Fig. 2. A) Change in interfacial surface tension (γ) with increasing concentrations of amphiphilic block copolymers PAA_{153}-*b*-$PnBA_{25}$ and PAA_{153}-*b*-$PnBA_{200}$, in comparison to sodium dodecyl sulfate (SDS). B) Interfacial elasticity for the same concentrations of block copolymers and SDS.

with plateau γ value of ~ 33 mNm^{-1} [75,83]. It has been reported that block copolymers display much lower CMCs than short-chain molecular surfactants such as SDS, and the CMC also decreases with increasing hydrophobic block length [59,60]. The specific CMCs of the polymers were not able to be clearly determined using interfacial tensiometry, because of slow relaxation times, and other methods such as fluorescence correlation spectroscopy may have been more appropriate to identify micelles [84]. The concentration range was also limited by the flotation performance envelope, where greater concentration resulted in little to no particle recovery (see Section 3.4). The observed lower surface activity associated with more hydrophobic copolymers has also been evidenced by Ghosh et al. [62], who examined the effect on surface activity/non-activity of a range of comonomer ratios, and found a critical transition point of hydrophilic/hydrophobic block length ratio when block copolymers became non-surface active. This transition effect was suggested to be a combination of the hydrophobic driven component and the image charge effects of parallel hydrophilic chains at the air–water-interface, where the addition of salt and resultant Debye screening resulted in a reduction of surface tension.

It has also been reported that the degree of hydrophilicity/hydrophobicity of the comonomers in a block copolymer play a role in the surface activity/non-activity, where weakly hydrophilic comonomers [58,85–87] and strongly hydrophobic comonomers [88] may micellise without adsorption to the air–water interface. The degree of image charge repulsion from hydrophilic polyions has also been found to destabilise block copolymers adsorbed at the air–water interface [61,62,89,90]. Similarly to Ghosh et al. [62], this image charge effect was observed by Eghbali et al. [90], when investigating the surface activity and micellisation of PAA_{150}-*b*-$PnBA_{100}$ polymer, where the addition of NaCl neutralised the image charge repulsion of PAA segments and lowered the CMC. Reduction occurred even at longer chain hydrophobic blocks, indicating that both image charge effects and hydrophobicity/block length were factors in surface activity. Consistent with Ghosh et al. [62], this work observed more significant surface activity for the less hydrophobic PAA_{153}-*b*-$PnBA_{25}$ than the PAA_{153}-*b*-$PnBA_{200}$, highlighting the relationship between decreasing hydrophobic chain length and its impact on surface tension reduction.

Fig. 2B presents the measured dilational elasticity (ε, mN·m^{-1}) for the three systems over the same concentration range. The dilational elasticity is a potentially important consideration in foaming systems or flotation operations where dynamic processes play a key role in determining system performance. As foams form and drain, higher elasticity values indicate a greater ability for the interface to remain stable to perturbations, as surface active species dynamically adsorb or desorb in response to surface area changes, potentially leading to lower bubble coalescence [23,91]. The elasticity values for PAA_{153}-*b*-$PnBA_{25}$ and PAA_{153}-*b*-$PnBA_{200}$ display differing magnitudes, although both show peaks at intermediate concentrations. The contrast in magnitude would be expected from the variance in their surface tension response. As elasticity is measured from the change in surface tension under oscillation, it is perhaps not surprising that the larger *MW*, more hydrophobic, polymer gives lower values, due to the lack of measured surface activity and slower diffusion of the larger copolymer. However, the general relationship between elasticity and concentration is characteristic of both low and high *MW* surface active molecules [90–95]. Since elasticity is a function of surface tension, it depends on the migration time of a molecule to diffuse from the bulk solution to the air–water surface upon expansion or contraction of the interface [94]. Therefore, as the surface-active molecules approach their respective CMCs, the total molecular diffusion time becomes fast and depletes the surface gradients created by the air–water interface perturbation [94]. Beyond this point, the elasticity begins to decrease as the formation of micelles competes with the diffusion of free surface-active molecules to replace those at the perturbed air–water interface [91–93].

Thus, the elasticity data in Fig. 2B suggests the CMC for the smaller *MW* PAA_{153}-*b*-$PnBA_{25}$ may be ~ 90 μM (correlating to the peak elasticity), although the surface tension still appears to reduce slightly beyond this point. The same observation is made for the PAA_{153}-*b*-$PnBA_{200}$ polymer, assuming the CMC occurs at the elasticity peak at ~ 11 μM, while the low values make interpretation difficult in this case. The fact the surface tension still decreases in both polymers beyond these points may be due to the slow conformational relaxation of these macromolecules and their tendency to form pre-micellar aggregates in the bulk phase [93–95]. The difference in apparent CMCs between the polymers would also agree with observations that longer chain hydrophobic block copolymers display lower CMCs, as well as slower conformational and diffusional exchange at perturbed air–water interfaces [91–93]. A peak in the SDS elasticity is not seen, as it is investigated at concentrations well below its CMC [75]. It presents an increase in elasticity, within expected magnitudes, due to its comparatively fast diffusional exchange and air–water interface relaxation times [95].

Other block copolymers such as pluronics, tri-block copolymers of poly(ethylene oxide) (PEO) and poly(propylene oxide) (PPO) used in paper deinking [96] and coal flotation operations [97], have also been investigated in regard to their dilational viscoelasticity. Noskov et al. [98] studied the viscoelasticity of PEO_{76}-*b*-PPO_{29}-*b*-PEO_{76}. They found a maximum spread film dilational elasticity of ~ 20 mN·m^{-1}, similar to those observed by the PAA_{153}-*b*-$PnBA_{200}$ system in Fig. 2B, although the lower molecular weight PAA_{153}-*b*-$PnBA_{25}$ displays elevated maximum dilational viscoelasticity of ~ 50 mN·m^{-1}. Whilst greater than those observed for pluronics by Noskov et al. [98], investigations of nanoparticle stabilised film elasticities of latex stabilised hexane/water interfaces with adsorbed block copolymers of poly(methyl methacrylate)-*b*-poly(2-(dimethylamino)ethyl methacrylate) have shown dilational viscoelasticity values in the range of 120–140 mN·m^{-1} [99].

3.2. Polymer-particle adsorption

Polymer-particle interactions of the two varying *MW* block copolymers were studied over a range of polymer concentrations, to investigate the impact of polymer structureon particle flocculation characteristics. The adsorption affinity of PAA_{153}-*b*-$PnBA_{25}$ and PAA_{153}-*b*-$PnBA_{200}$ for the surface of $Mg(OH)_2$ particles is presented in Fig. 3, where initial calibrations (UV-Vis absorption vs polymer concentration) with reference polymer solutions can be found within the ESM (Fig. S3A-B). Here, a wavelength of 304 nm was selected from the measured 300–350 nm range as the peak maximum. The linear correlation

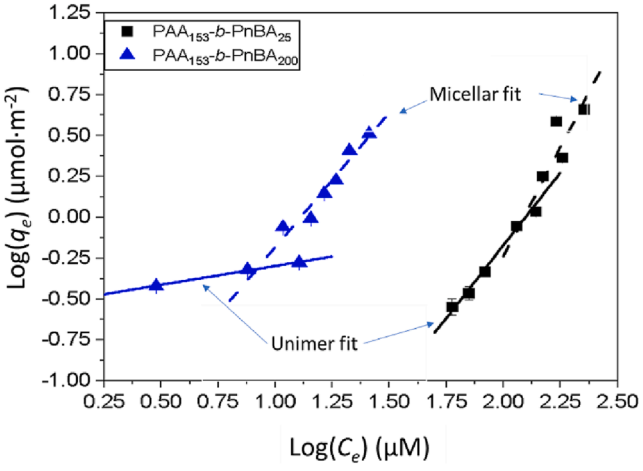

Fig. 3. Adsorption isotherms for amphiphilic block copolymers PAA_{153}-*b*-$PnBA_{25}$ and PAA_{153}-*b*-$PnBA_{200}$ onto $Mg(OH)_2$ particles, in terms of equilibrium concentration (C_e), fitted to a two region Freundlich model. Here, C_e* is indicated by the unimer-micellar fit intercept, showing the critical transition concentration between unimer and micellar adsorption regimes.

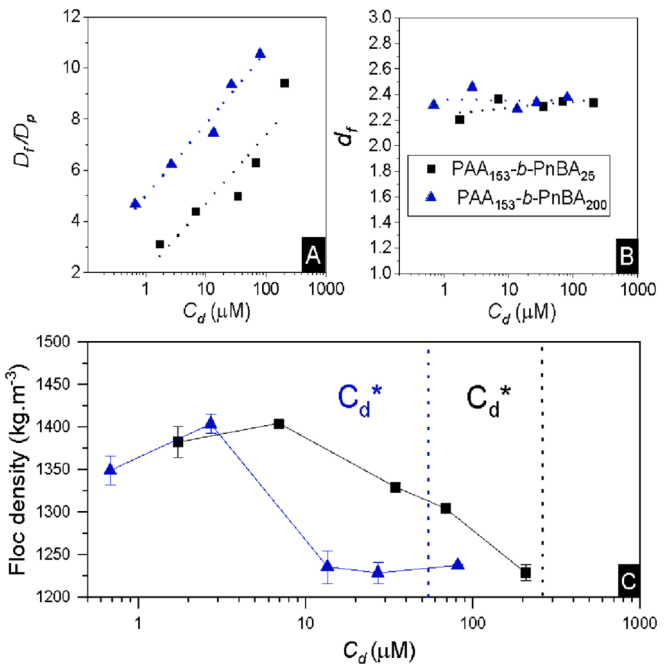

Fig. 4. A) Change in the ratio of the smallest repeating floc unit diameter (D_f) to the primary particle diameter (D_p) with increasing block copolymer concentration determined through static light scattering. B) The change in fractal dimension (d_f) with increasing block copolymer concentration determined through static light scattering. C) Floc density with increasing block copolymer concentration determined via Eqn. 3. Symbols as per legend in B in all cases.

between dosed concentration, C_d, and equilibrium supernatant concentration, C_e, is also shown within the ESM (Fig. S4A).

There is a distinct difference in the adsorption behaviour between the PAA_{153}-*b*-$PnBA_{25}$ and PAA_{153}-*b*-$PnBA_{200}$ systems. Fig. 3 presents the Freundlich adsorption isotherms, indicating a unimer adsorption regime and micellar adsorption regime for both block copolymer systems. The two adsorption isotherms describe the changing surface adsorption density (Log q_e) of the polymers on the $Mg(OH)_2$ surfaces, with increasing logarithmic supernatant equilibrium concentration (Log C_e). Firstly, there is the initial electrostatic adsorption and relaxation of unimer block copolymers onto the particle surface driven by the PAA block, followed by potential relaxation and hydrophobic adsorption of the hydrophobic PnBA tails to the charge neutralised sites on the particle surface. The processes, which occur below the block copolymer CMC, reduce the free energy of the system [34,46,100]. Secondly, at higher concentration of added polymer, there is micellar adsorption of block copolymers to the surface, increasing the mass of polymer on the surface to a significantly greater degree.

The mechanistic transition from unimer to micellar adsorption is indicated by the transition of both *1/n* values for the block copolymers in the steeper right-hand isotherms being greater than 1 (see Table 1). Values for $1/n > 1$ suggest increasing adsorption affinity with concentration. As greater block copolymer adsorption occurs on the $Mg(OH)_2$ surface, the adsorption intensity of block copolymers increases, inferring greater van der Waals attraction to the hydrophobic tails[101,102]. The two block copolymers differ in their *1/n* values, with the higher molecular weight block copolymer showing a considerable increase in adsorption intensity between the isotherm regimes. This suggests that the adsorption affinity increases with increasing concentration of the block copolymer on the surface and that the exponential adsorption is driven by both enthalpic and entropic components due to the larger hydrophobic tail group. Conversely, for the lower *MW* block copolymer, the *1/n* value transitions from < 1 (as normal for surfactants) to > 1, suggesting the transition from enthalpic dominance in the left-hand isotherm to entropic dominance in the right-hand isotherm. This mechanism is supported by the enthalpically favourable hydrophobic attraction of the PnBA tails of the copolymer in the bulk solution and those on the particle surface, indicated by the linear increase in the percentage of polymer in bulk solution with surface adsorption (see ESM Fig. S4B) [45].

The unimer and micellar adsorption regimes for the lower *MW* PAA_{153}-*b*-$PnBA_{25}$ block copolymer have much closer adsorption intensity values (*1/n*) than their greater *MW* counterpart (PAA_{153}-*b*-$PnBA_{200}$). However, both adsorption regime intensities are larger than the PAA_{153}-*b*-$PnBA_{200}$ equivalents. At the unimer-micellar adsorption transition concentration (C_e*), located at the intercept of the two isotherms, there is a stark increase in the greater *MW* PAA_{153}-*b*-$PnBA_{200}$ block copolymer adsorption intensity. It should be noted that for both block copolymer systems, their C_e* values align with the dilatational viscoelasticity peaks in Fig. 3B, which is likely related to the block copolymer CMCs [94]. The greater *MW* PAA_{153}-*b*-$PnBA_{200}$ block copolymer and lower *MW* PAA_{153}-*b*-$PnBA_{25}$ block copolymer have C_e* values of 8 μM and 119 μM respectively, as shown in Table 1 (along with other Freundlich isotherm fitting constants). These parameters were then related back to the dosed concentration using the C_d vs C_e plot (see ESM Fig. S4A) and the equivalent dosed transitional C_d* block copolymer concentrations are shown in Table 1, highlighting close correlation to the observed inflection in dilational viscoelasticity in Fig. 2B.

Although the dilation and adsorption experiments conducted in this study involved investigations of air–water and solid-water interfaces respectively, small deviations between the CMC concentrations estimated from dilational and adsorption measurements could be due to differences in the degree of deprotonation of the PAA carboxyl functional groups. PAA is known to undergo greater dissociation at higher pH levels, and as the dilational viscoelasticity studies in Section 3.1 were completed without the presence of $Mg(OH)_2$ that provides pH buffering, it is reasonable to expect a low degree of deprotonation at pH 7 (~30%). Swift et al. [103] observed that PAA chains with a molecular weight of < 16.5 kDa do not readily protonate compared to their higher *MW* counterparts due to thermodynamic arguments around short-chain hydrogen bond formation in acidic solutions. Therefore, a greater degree of deprotonation may be occurring in the system observed in this study (PAA chains ~ 11 kDa), promoting stronger similarities between dilational and adsorption measurements.

At the unimer-micellar adsorption transition point, the adsorption densities of the lower *MW* PAA_{153}-*b*-$PnBA_{25}$ block copolymer are greater than the larger *MW* PAA_{153}-*b*-$PnBA_{200}$ block copolymer; with q_e* values of ~ 0.92 and ~ 0.48 μmol·m^{-2} respectively. There are two factors influencing these q_e* values. Firstly, as the lower *MW* block copolymer has a shorter chain length, it can more easily conform and relax to the $Mg(OH)_2$ particle surface. Also, the smaller hydrophobic chain will provide lower steric barriers to further adsorption of block copolymers on the $Mg(OH)_2$ surface [100]. Furthermore, the unimer-micellar adsorption transition point occurs at a much greater concentration due to the comparative entropic stability of the lower *MW* block copolymer. This results in a greater concentration gradient of block copolymer in

Table 1
Freundlich adsorption isotherm coefficients, k_f and *n*, with corresponding coefficients of determination for amphiphilic copolymers PAA_{153}-*b*-$PnBA_{25}$ and PAA_{153}-*b*-$PnBA_{200}$ above and below their estimated critical micelle concentrations calculated from the data in Fig. 3.

Isotherm value	PAA_{153}-*b*-$PnBA_{25}$		PAA_{153}-*b*-$PnBA_{200}$	
	Unimer	Micellar	Unimer	Micellar
Freundlich R^2	0.99	0.79	0.99	0.97
k_f (μmol·m^{-2})	1.8×10^{-4}	2.5×10^{-6}	0.296	0.015
1/n	1.78	2.69	0.23	1.65
q_e* (μmol·m^{-2})	~0.92		~0.48	
C_e* (μM)	~119		~8	
C_d* (μM)	~269		~54.7	

bulk solution to drive adsorption onto the $Mg(OH)_2$ particle surface.

Additionally, the associated van der Waals attraction between the bulk solution and adsorbed PnBA tails is reduced due to the lower molecular weight, which is indicated by the greater *1/n* values compared to both regimes for the greater *MW* block copolymer [59,60,91–93,95]. It is lastly noted that previous work by the current authors [57] investigated the adsorption densities of SDS onto $Mg(OH)_2$, again through its monolayer and bilayer adsorption regimes using Freundlich adsorption isotherms. The monolayer-bilayer transition concentration was found to have a q_e* value of 0.11 μmol·m^{-2}, which is lower (although in the same region) than those observed for the block copolymers in this work, inferring close conformation of the polymers in the current case on the surface of the particles (noting these are both relatively small *MW* polymers).

3.3. Floc structure characterisation

The flocculation characteristics of the two block copolymers were investigated using SLS, with Fig. 4A showing an increase in the ratio of the minimum repeating floc size to primary particle size (D_f/D_p) with increasing dosed copolymer concentration. Consistent with its greater adsorption density at low concentrations, the more hydrophobic PAA_{153}-*b*-$PnBA_{200}$ produces significantly larger flocs. It is assumed the charged PAA segments cause local neutralisation of the $Mg(OH)_2$ surface which could promote charge-patch flocculation, while the hydrophobic PnBA segments may extend away from the surface and promote bridging flocculation [45].

Determined fractal dimensions, d_f (see ESM Fig. S5 for raw *logI(Q)* with respect to *logQ* data for both polymers) for varying dosed concentrations, are shown in Fig. 4B. The d_f values are approximately constant with increasing block copolymer concentrations for both systems, displaying values in the range of 2.2–2.4. For high charge density polymeric flocculants (100% charge density) of small to intermediate *MW*, similar high fractal dimensions have been previously recorded. Zhou and Franks [37] measured fractal dimensions of ~ 2.7 for a homopolymer poly(diallyldimethylammonium chloride) (PDADMAC) used to flocculate silica particles, however for kaolin flocculated with polyaluminium chloride, values were in the range of 2.1–2.3 [104]. Fractal dimension is a function of polymer charge density, particle concentration and polymer conformation and these factors can affect the flocculation mechanism [105]. These mechanisms have been modelled by various authors [106,107] and generally quantify fractal dimensions of 2.2–2.4 as following an aggregation mechanism between diffusion limited particle-cluster aggregation and reaction limited cluster–cluster aggregation [108]. Additionally, Bushell et al. [105] reported that bridging flocculation systems can display fractal dimensions of 1.75–2.5, which indicates an area of uncertainty regarding flocculation mechanism for structures of these intermediate fractal dimensions.

In fact, in addition to the PDADMAC homopolymer, Zhou and Franks [37] investigated a copolymer of PDADMAC and polyacrylamide with a cationic charge density of 40% and found that the flocculation mechanism was likely a combination of charge patch and bridging flocculation mechanisms. This dual functionality has interesting implications for the block copolymer systems, as there is little known about their flocculation mechanisms or effect on fractal dimension. It is also noted that in previous work by the current authors [26], very high *MW* (10^6 g·mol^{-1}) statistical copolymers of PAA and poly(acrylamide) (PAM) of 30% and 40% charge density were used to flocculate similar $Mg(OH)_2$ suspensions. This work reported fractal dimensions consistent with open, porous bridging mechanisms of 2.07–2.09 (giving computed floc densities of ~ 1045–1049 kg·m^{-3}).

Calculated floc densities for the block copolymers are given in Fig. 4C (See ESM Section S3 and Eqns. S4 and S5 from previous work [57]). Fig. 4C indicates that the flocs display relatively large particle agglomeration densities (correlated to their high fractal dimensions) compared with traditional reaction limited cluster–cluster flocculation [106,107]. Interestingly, there is also a clear decrease in floc density with increasing polymer concentration (and associated floc size). This change appears to lead to a transition to a plateau value at ~ 1230 kg·m^{-3} for aggregates using the larger *MW* PAA_{153}-*b*-$PnBA_{200}$, whereas the flocs from the smaller copolymer have a more gradual decrease in density that also approaches ~ 1230 kg·m^{-3}. The density plateau for the more hydrophobic block copolymer occurs at approximately the unimer-micellar transition concentration, C_d* (although, onset appears slightly before the transition point). Nevertheless, this result does suggest that reduction in density occurs with the formation of pseudo-bridging flocculation through micellar intermediates between particles, which is schematically illustrated in Fig. 5.

O'Shea et al. [45] also noted that P(AA-*co*-BA)-*b*-PNIPAM block copolymers could adsorb at particle surfaces, facilitating flocculation with micellar intermediates between particles, using a combination of charge-patch, charge neutralisation and hydrophobic attraction mechanisms. These hydrophobic blocks have much shorter chain lengths than traditional bridging flocculants, while the adsorption of high charge density hydrophilic blocks provides electrostatic charge neutralisation, reducing the electrical double layer repulsion between particles [100]. The transition to plateau floc densities of ~ 1230 kg·m^{-3} at lower concentrations of the greater *MW* system likely indicates a pseudo-bridging flocculation mechanism. For the lower *MW* polymer, there is a gradual transition to this mechanism, as larger proportions of copolymer are entropically driven to adsorb to the particle surface with increasing concentration. Whilst the unimer-micellar transition occurs slightly below the proposed unimer-micellar transition point concentration (C_d* in Table 1) for PAA_{153}-*b*-$PnBA_{200}$ block copolymer. It is known that large thermodynamically unstable hydrophobic block copolymers form pre-micellar aggregates before full micelles [91,93,95]. Thus, it is possible that the adsorption of the pre-micellar aggregates lowers the observable transition concentration below the CMC.

3.4. Sedimentation and flotation performance

Fig. 6A presents the change in zonal settling rate with initial dosed block copolymer concentrations. For both systems, there is a clear increase in zonal settling rate from the non-flocculated baseline. The larger PAA_{153}-*b*-$PnBA_{200}$-$Mg(OH)_2$ flocs have a distinctly greater settling rate at lower dosed concentrations than the lower *MW*, less hydrophobic, system. Initially, for the more hydrophobic longer copolymer, there is a plateau sedimentation performance below the unimer-micellar transition (dosed concentration C_d* highlighted in Fig. 6A). Above this concentration, there is a significant increase in zonal settling rate. For the PAA_{153}-*b*-$PnBA_{25}$-$Mg(OH)_2$ system, however, there is a more gradual increase in floc settling rates, inferring differences in floc structure from the lower degree of polymer hydrophobicity, as discussed in relation to Fig. 4. Fig. 6B presents images of settling tubes showing the flocs formed with increasing dosed concentration for the more hydrophobic PAA_{153}-*b*-$PnBA_{200}$, where the change in aggregate size is clearly visible. Visual evidence of the differences in aggregate size between the polymers is given in Fig. 6C-D, with microscopy images of extracted samples at concentrations below and above the unimer-micelle transition point. Here, the larger floc sizes are evident in the micelle region (Fig. 6Cii and 6Dii) correlating to the faster settling velocities, while the larger *MW* polymer also displays much greater aggregate sizes than the smaller polymer (noting the difference in size of the image scale bars).

The change in zonal settling rate is function of a number of factors, especially in hindered settling systems. The sedimentation dynamics have been found to be sensitive to floc size when inter-aggregate packing density was lower than the intra-aggregate packing density, where flow around the flocs was free and not restricted by floc-floc spacing permeability [26,71,109]. Fig. 6C indicates that the two-block copolymer aggregate suspensions in this work have more compact floc densities than traditional flocculation agents previously investigated [26]. This difference suggests that for the block copolymer systems floc size

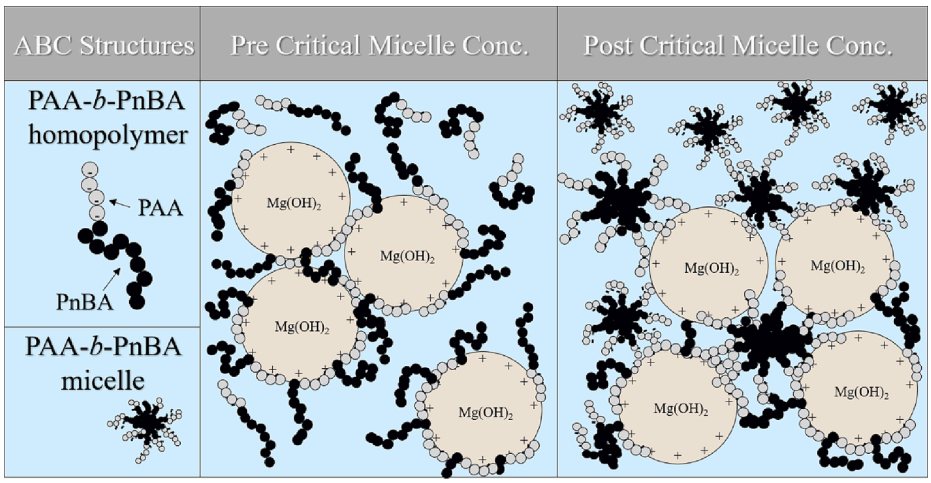

Fig. 5. Illustration of the change in adsorption and flocculation mechanisms pre and post critical micelle concentrations (CMC) of the amphiphilic block copolymers.

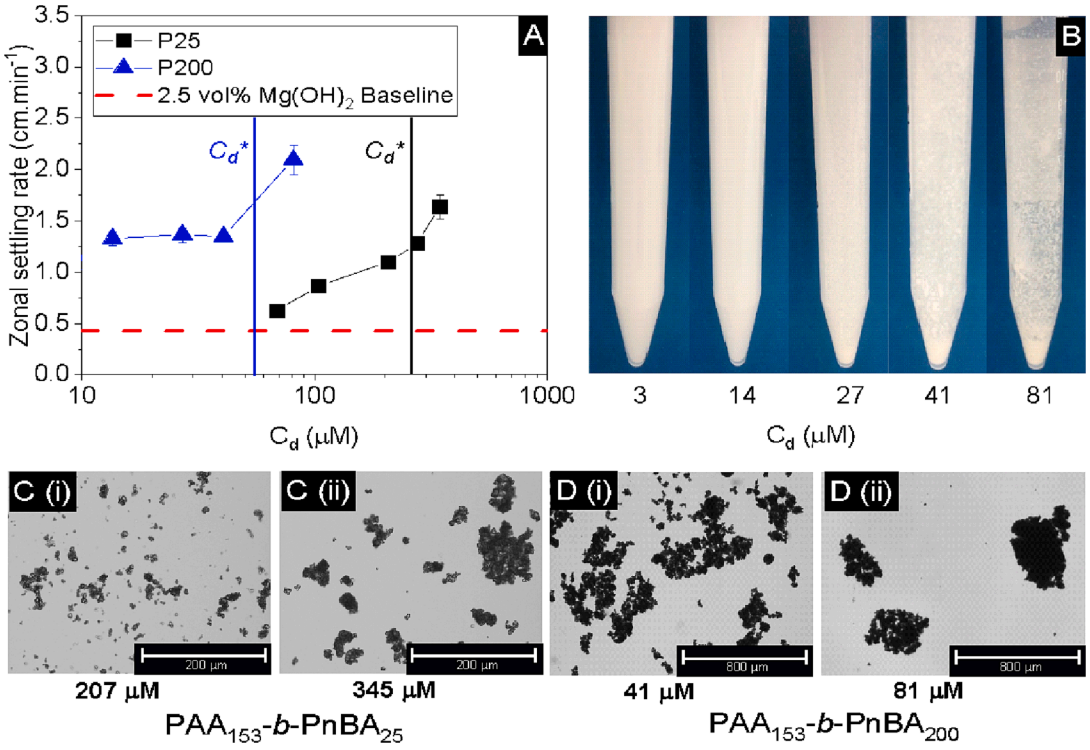

Fig. 6. A) Measured sedimentation rate of $Mg(OH)_2$ flocculated with amphiphilic block copolymers PAA_{153}-*b*-$PnBA_{25}$ and PAA_{153}-*b*-$PnBA_{200}$. B) Images of the flocs, within settling tubes, with increasing concentrations of PAA_{153}-*b*-$PnBA_{200}$ block copolymer. C) Single element microscopy images of PAA_{153}-*b*-$PnBA_{25}$ $Mg(OH)_2$ flocs at (i) 207 μM and (ii) 345 μM added copolymer. D) Single element microscopy images of PAA_{153}-*b*-$PnBA_{200}$-$Mg(OH)_2$ flocs at (i) 41 μM and (ii) 81 μM added copolymer.

and density are dominant, as inter-aggregate packing allows for substantial flow around the structures, reducing hindering affects when compared to large bridging flocculation systems [25,26]. However, drag and shape effects are likely influential on the zonal settling rates, with suspension permeability being effectively less important than in highly porous bridging flocculation systems due to lower inter-aggregate packing density than intra-aggregate packing between the floc structures [64,110]. This structural difference in the flocs implies that floc-floc interaction effects are also less important, where it has been found in previous investigations that larger flocs are more influential on zonal settling rates due to netting effects [26,33,111,112].

As an alternative to sedimentation, flotation is being increasingly considered for dewatering applications, as it is a high-rate process with much greater space efficiency [57]. To investigate the efficacy of the block copolymers as flotation agents, the mass percentage of recovered $Mg(OH)_2$ during batch flotation operations with dosed block copolymers is displayed in Fig. 7A. Here, data is also given for a third polymer of intermediate hydrophobic chain length (PAA_{153}-*b*-$PnBA_{100}$) in addition to the smaller and larger hydrophobic block polymers previously characterised. Flotation performance was also benchmarked against recovery using SDS as a collector, determined in a previous study [57]. The SDS appears to outperform all three block copolymer systems in terms of mass recovery of $Mg(OH)_2$. For SDS the recovery plateaus at 93% recovery, while for the polymer systems the greatest recovery occurs with the largest *MW* PAA_{153}-*b*-$PnBA_{200}$ (peaking at 52%), where the smallest hydrophobic block polymer performs very poorly (~30% maximum

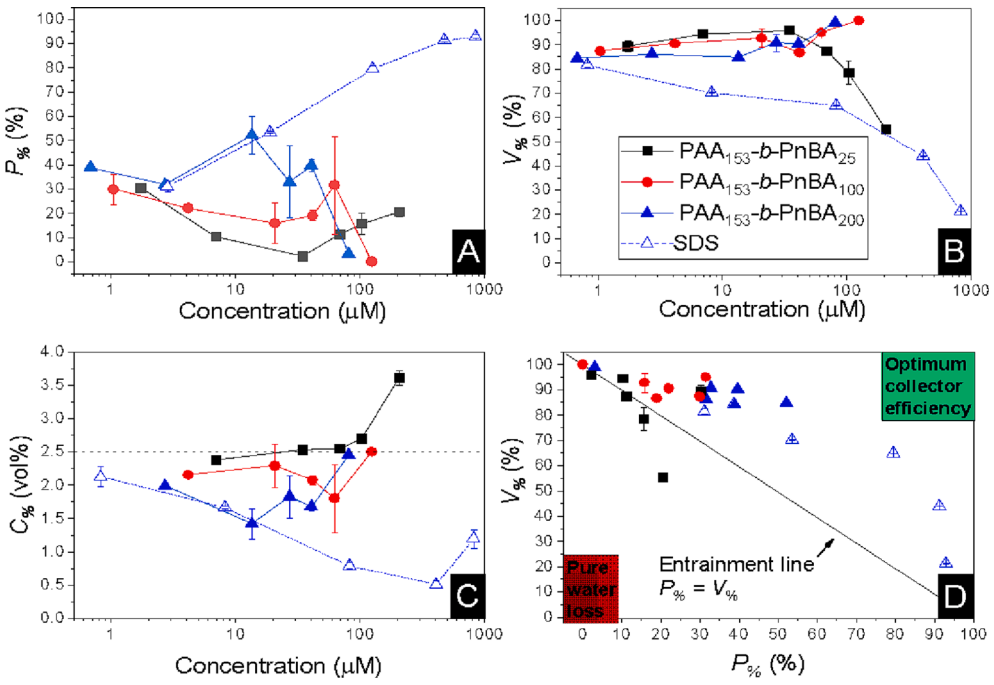

Fig. 7. A) Percentage of $Mg(OH)_2$ recovered using amphiphilic block copolymers PAA_{153}-*b*-$PnBA_{25}$, PAA_{153}-*b*-$PnBA_{100}$ and PAA_{153}-*b*-$PnBA_{200}$ in comparison to SDS surfactant, all with 98 μM MIBC. B) Remaining suspension volume after flotation operations as a function of concentration. C) Residual bulk concentration of $Mg(OH)_2$ remaining in the cell post-flotation. D) Comparison of remaining suspension volume as a function of the percentage of $Mg(OH)_2$ recovered. Symbols as per legend in B in all cases.

recovery), and the intermediate *MW* PAA_{153}-*b*-$PnBA_{100}$ recovers an intermediate amount (~32% max).

The flotation recovery trends are consistent with expectations of the degree of hydrophobisation that the polymers impart onto the $Mg(OH)_2$ aggregates upon adsorption. It is clear that the small hydrophobic block of the PAA_{153}-*b*-$PnBA_{25}$ polymer is almost completely insufficient to enhance aggregate contact angles to promote bubble attachment. It is also noted that, at least for the intermediate and large hydrophobic block polymers, maximum recovery occurs at a dosed concentration below expected micelle transition. Above transition, performance reduces markedly, as the micelles remove the ability for the polymers to modify the degree of wetting of particle aggregates, due to the formation of charged corona of PAA blocks, much like a surfactant system [8,9,41,38,113].

The mass of water remaining in the flotation cell post-flotation is shown in Fig. 7B as a comparison to particulate recovery (where both are needed for an efficient dewatering operation). An interesting observation is the significant water losses associated with the SDS and lowest *MW* PAA_{153}-*b*-$PnBA_{25}$. Fig. 2A indicates that SDS and PAA_{153}-*b*-$PnBA_{25}$ collectors have the greatest air–water interfacial surface activity, with corresponding largest dilational elasticities (Fig. 2B). Excess water losses, compared with the greater *MW* system, are likely related to the increased foamability, as well as small contributions from the improved foam stability. Foams with higher interfacial elasticity have shown an increased ability to dissipate energy from local shear stresses, preventing film rupture and enhancing resistance to disproportionation, through adverse capillary pressure gradients. This occurs for foams with disperse bubble size distributions, although, not to the extent of particle stabilised foams which can sterically resist film drainage [23]. The small rise in $Mg(OH)_2$ recovery at higher dosed concentrations for the lower *MW* block copolymer is likely related to the corresponding increased water loss due to entrainment within an overly stable foam film, much like the SDS system. This has been observed by Said et al.[40] where their froth flotation foam acted to filter hydrophilic particles during drainage at greater foam residence times. Indeed, because of the presence of MIBC as the primary foaming agent, additional stabilising effects from collector interactions at air–water interfaces appears to reduce true flotation performance, rather than enhance it in this case. There are lower rates of water loss when considering the intermediate and most hydrophobic copolymers, which is likely due to their much lower surface activity as reported for other hydrophobic chain length polymers [61,62] and shown in Fig. 2A.

The compound effects of the relative $Mg(OH)_2$ recovery and water retained in the flotation cell are summarised in Fig. 7C, which displays the residual cell concentration (vol.%) post flotation as a function of dosed collector concentration. Fig. 7D shows the relative mass of particles recovered as a function of water remaining in the flotation cell, which is compared to an entrainment line ($P_{\%} = V_{\%}$). It is apparent that when considering the residual cell concentration, SDS appears to reduce the flotation cell concentration most effectively, which is also reflected in Fig. 7D, and indicates that a much greater mass of particles was recovered than water lost from the flotation cell. However, at higher concentrations, enhanced particle recoveries were also associated with greater degrees of water loss from the cell, reducing the overall efficiency. At lower concentrations, the largest PAA_{153}-*b*-$PnBA_{200}$ polymer actually performed comparatively better than SDS (in terms of the ratio of recovery to water retainment) and similar in terms of reduction in dispersion concentration, before reducing significantly above the unimer-micellar transition concentration. Such comparisons highlight that a number of factors need to be correlated to understand the true operational efficiency of collectors for dewatering, rather than just total collection percentage.

The lowest *MW* polymer also gave some interesting performance characteristics, as Fig. 7C shows that the residual cell concentration increases above the initial 2.5 vol% $Mg(OH)_2$ suspensions, inferring there is, in fact, a greater mass of water lost than of $Mg(OH)_2$ aggregates. This result is likely due to the high surface activity and thus foamability of the PAA_{153}-*b*-$PnBA_{25}$, as well as its relatively poor adsorption characteristics (leading to high relative concentrations able to interact with foam interfaces). It also suggests that the small increase in recovery at higher polymer concentration doses is from entrainment rather than hydrophobic interactions. Again, the intermediate *MW* PAA_{153}-*b*-$PnBA_{100}$ block copolymer had an intermediate performance by all four metrics in comparison.

The collection efficiency factor (Eqn. (2)) allows quantification of the overall dewatering ratios of the three polymers and SDS, which can be related to their adsorption and flocculation characteristics. Fig. 8A shows the collection efficiency factors for the three polymers and SDS,

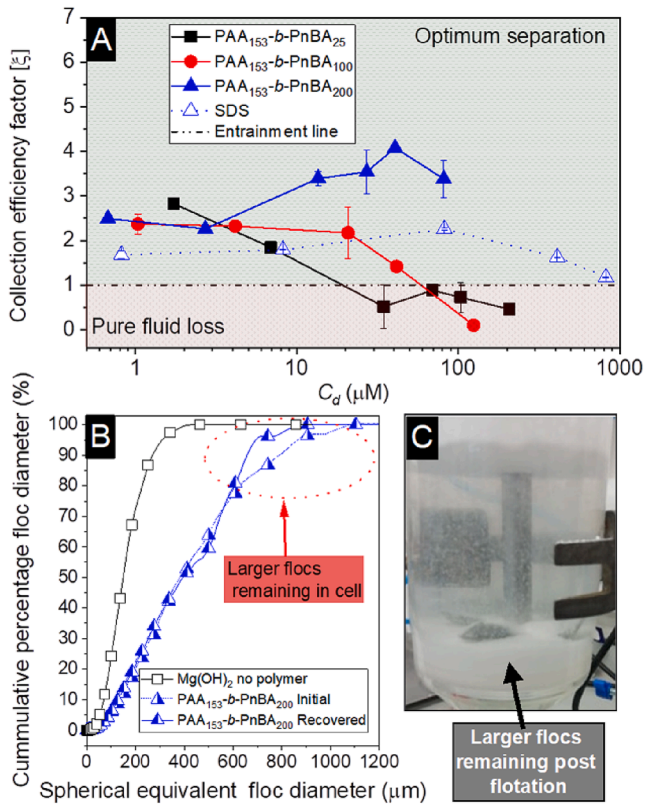

Fig. 8. A) The collection efficiency factor calculated using Eqn. (2) as a function of dosed concentration of block copolymer and SDS. B) Data showing the cumulative frequency distribution of particle size populations for $Mg(OH)_2$ in the batch flotation cell agitated at 250 rpm for 5 min, in comparison to 14 μM of amphiphilic block copolymer PAA_{153}-*b*-$PnBA_{200}$ agitated 250 rpm for 5 min, and the size distribution of block copolymer-$Mg(OH)_2$ flocs extracted during flotation in the foam phase. C) Image of flocculation cell post flotation.

again as a function of dosed concentration. The same mechanistic observations are made regarding Fig. 7C and 7D, where the entrainment line is represented by $\xi = 1$. When $\xi < 1$ there is a greater mass of water being recovered than $Mg(OH)_2$ particles and when $\xi > 1$ there is successful dewatering occurring. Effectively, the greater the magnitude of ξ, the greater the collection efficiency. In work with SDS [57], it was found that the greatest ξ values occurred when the surface adsorption density reached monolayer coverage. Beyond this point (as a bilayer of SDS began to form) the performance decreased markedly, as shown in Fig. 8A, where $Mg(OH)_2$ recovery was mainly through liquid entrainment rather than adsorption interactions (reflected by the collection factor approaching $\xi = 1$).

The collection efficiency factor in Fig. 8A helps to accentuate the flotation trends observed in Fig. 7, where the increase in relative performance of the most hydrophobic PAA_{153}-*b*-$PnBA_{200}$ polymer over all other systems, including SDS, is now evident at low to moderate dosed concentrations, until the unimer-micellar transition ($C_d \sim$ 30–50 μM). The limitation of flotation using the block copolymers appears to be a balance of their hydrophobising capacity (which is prohibited beyond micellisation) and the resultant floc size, which can hydrodynamically limit $Mg(OH)_2$ recovery. This is ultimately highlighted when comparing the PAA_{153}-*b*-$PnBA_{200}$ performance directly with SDS, where the PAA_{153}-*b*-$PnBA_{200}$ system has much greater collection efficiency and is likely due to its superior hydrophobising capacity, granted by a much longer hydrophobic chain length and low surface activity, reducing excess water loss.

It is also important to consider the competing influence of flocculation on flotation. As the dosed concentration of PAA_{153}-*b*-$PnBA_{200}$ increases, there is an increase in floc size (see Fig. 6-D(ii)) to a much greater degree than PAA_{153}-*b*-$PnBA_{25}$, inferring there may be increasing hydrodynamic restrictions preventing mass transfer of flocs to the foam phase [114]. The decreased particle recovery at these higher concentrations provides a lower degree of stratification at the air–water interfaces in the foam, reducing the effect of the steric barrier that prevents fluid draining from the foam lamella back into the flotation cell [23,24]. Additionally, increased floc sizes in flotation operations have also been reported to increase film piercing, which may exacerbate drainage to the point of destabilising foam structures resulting in collapse [67].

The hydrodynamic restrictions of the flotation operation were further investigated by assessing the impact of block copolymer flocculation on flotation performance. Here, the best particle recovery system was selected (PAA_{153}-*b*-$PnBA_{200}$ block copolymer system at 14 μM dosed concentration) as this allowed for the greatest proportion of particles to compare before and after flotation operation, rather than the greatest collection efficiency factor. The cumulative size distributions of flocs were characterised (using single-element automated microscopy) from samples taken in the flotation cell before flotation commenced, as well as from the froth phase post flotation, and are compared to non-flocculated particles in Fig. 8B.

As observed for the sedimentation tests, the hydrophobic block copolymer effectively flocculates the particles in the flotation cell, with size increasing significantly across the entire PSD. Comparing the PSDs from the collected froth and the initial mixed dispersion can help establish the hydrodynamic limitations of using the block copolymers as collectors. Noticeably, the d_{10} and d_{50} values are very similar pre and post-flotation. However, there is a larger difference in d_{90} values, with pre-flotation showing a d_{90} spherical equivalent floc diameter of around 800 μm, whereas post-flotation samples from the separated froth indicate a d_{90} spherical equivalent floc diameter in the order of 650 μm. This difference indicates that flotation using flocculating block copolymers as collectors effectively targets fines and intermediate particle sizes, pushing limits of coarse particle flotation when considering traditional bubble attachment mechanics [8]. Due to the porous and fractal nature of flocs, it is possible that floc structures may interact with or even entrain multiple bubbles in floc-bubble aggregates which have been observed by Zhang et al. [4] when using humic acid to float TiO_2. In the case of floc-bubble aggregates, the fractal density of the aggregate is further reduced, allowing buoyant forces to overcome gravitational forces, and the bubble rise velocity is reduced which impacts interceptional effects benefiting finer aggregates [10]. As bubbles are entrained in floc structures it is likely that detachment due to radial inertia is reduced, if not eliminated, improving the hydrodynamic phase transport effectiveness [11]. It should be noted that this would likely be detrimental for systems requiring selectivity.

Further qualitative assessment is reflected in Fig. 8C, which shows an image of the flotation cell post-flotation, where it is evidenced visually that larger flocs remain in the flotation cell that have settled and consolidated on the base of the cell. This suggests that the block copolymer collectors produce flocs of sizes above hydrodynamic limits for flotation. Thus, to compensate, these larger flocs could be targeted using a subsequent sedimentation stage, which is often built into flotation cells as waste sludge outlets [115]. Therefore, it is suggested that the best utilisation of these charged block copolymers would be in dual flotation-sedimentation operations.

4. Conclusions

Amphiphilic block copolymers of poly(acrylic acid)-*b*-poly(*n*-butyl acrylate), with consistent hydrophilic poly(acrylic acid) chain length and varying hydrophobic chain length, were investigated as potential dual flocculant-collectors for combined flotation-sedimentation dewatering operations targeting $Mg(OH)_2$ radioactive waste removal. Various techniques characterised polymer behaviour at the air–water

interface and their adsorption onto $Mg(OH)_2$ particles. Longer hydrophobic chain lengths exhibited reduced surface activity, resulting in decreased foamability, water entrainment, and dilational elasticity. The unimer-micellar adsorption transition points were determined based on viscoelastic properties and confirmed by particle adsorption studies. The largest molecular weight block copolymer displayed significant changes in floc density as the dosed concentration increased into the micellar adsorption region, indicating a structural shift facilitated by micellar intermediates and pseudo-bridging flocculation. The polymers' application as a flocculation agent was assessed through particle sedimentation, with particles adsorbed by the larger molecular weight polymer settling at notably faster rates, correlated with their larger aggregate sizes (particularly beyond the micellar transition point). Their efficacy as polymeric collectors was also examined, and the largest molecular weight block copolymer exhibited superior collection efficiency, even outperforming the traditional surfactant SDS, below its micellar adsorption transition point. However, hydrophobisation of $Mg(OH)_2$ particles and subsequent collection was hindered beyond the transition of low surface energy micelles due to the lack of exposed hydrophobic blocks. Analysis of flotation cell particle size distributions suggested hydrodynamic hindrance of recovery due to the high bubble detachment energies associated with the largest floc sizes, thus, combined flotation-sedimentation operations have significant potential as unfloatable aggregates would settle quickly in a subsequent clarification step. In summary, the pseudo-bridging flocculation regime demonstrated superior settling rates prior to flotation, while post-flotation sedimentation is expected to yield the most substantial reduction in solids cell concentration, indicating a promising application of these amphiphilic block copolymers for rapid dewatering of radioactive and other mineral wastes.

CRediT authorship contribution statement

Alexander P.G. Lockwood: Conceptualization, Investigation, Methodology, Data curation, Formal analysis, Writing – original draft. **Georgina Wadsley:** Investigation, Data curation, Formal analysis, Writing – review & editing. **Nicholas J. Warren:** Formal analysis, Validation, Writing – review & editing. **Jeffrey Peakall:** Formal analysis, Validation, Writing – review & editing. **Grant B. Webber:** Methodology, Formal analysis, Writing – review & editing. **Erica J. Wanless:** Formal analysis, Writing – review & editing. **Dominic Rhodes:** Project administration, Writing – review & editing. **Martyn Barnes:** Project administration, Writing – review & editing. **David Harbottle:** Project administration, Formal analysis, Writing – review & editing. **Timothy N. Hunter:** Conceptualization, Methodology, Investigation, Validation, Funding acquisition, Writing – review & editing.

Declaration of Competing Interest

The authors declare that they have no known competing financial interests or personal relationships that could have appeared to influence the work reported in this paper.

Data availability

Data will be made available on request.

Acknowledgements

The authors would like to thank the Engineering and Physical Sciences Research Council (EPSRC) U.K. and Sellafield Ltd for funding this research through the Centre for Doctoral Training in Next Generation Nuclear (NGN-CDT) [EP/L015390/1]. GBW and EJW also acknowledge the funding support from the Australian Research Council for the ARC Centre of Excellence for Enabling Eco-Efficient Beneficiation of Minerals, grant number CE200100009. Thanks is given to Stuart Micklethwaite and the Leeds Electron Microscopy and Spectroscopy (LEMAS) Centre for their assistance and guidance with the scanning electron microscope experiments. The authors would finally like to thank the reviewers for taking time to review this article.

Appendix A. Supplementary data

Supplementary data to this article can be found online at https://doi.org/10.1016/j.seppur.2023.124387.

References

[1] L. Chang, Y. Cao, G. Fan, C. Li, W. Peng, A review of the applications of ion floatation: Wastewater treatment, mineral beneficiation, and hydrometallurgy, RSC Adv. 9 (35) (2019) 20226–20239, https://doi.org/10.1039/C9RA02905B.
[2] R.A. Hyde, D.G. Miller, R.F. Packham, W.N. Richards, Water clarification by flotation. Journal (American Water Works Association), 69(7), 369-374, 1977. http://www.jstor.org/stable/41268991.
[3] M.Y. Prajitno, S. Tangparitkul, H. Zhang, D. Harbottle, T.N. Hunter, The effect of cationic surfactants on improving natural clinoptilolite for the flotation of cesium, J. Hazard. Mater. 402 (2021), 123567, https://doi.org/10.1016/j.jhazmat.2020.123567.
[4] H. Zhang, Y.K. Kim, T.N. Hunter, A.P. Brown, J.W. Lee, D. Harbottle, Organically modified clay with potassium copper hexacyanoferrate for enhanced Cs+ adsorption capacity and selective recovery by flotation, J. Mater. Chem. A 5 (30) (2017) 15130–15143, https://doi.org/10.1039/C7TA03873A.
[5] S. Gong, H. Wang, S. Zhang, S. Jiang, X. Zhao, Q. Hou, Evaluating the Applicability of High-Speed Air Flotation Technology for Water Supply: A Case Study in Tianjin Binhai New Area. Separations. 9(11), 362, 2022. 10.3390/separations9110362.
[6] M.R. Teixeira, M.J. Rosa, Comparing dissolved air flotation and conventional sedimentation to remove cyanobacterial cells of Microcystis aeruginosa: Part I: The key operating conditions, Sep. Purif. Technol. 52 (1) (2006) 84–94, https://doi.org/10.1016/j.seppur.2006.03.017.
[7] D. Osborne, J. Euston, Value of the Jameson Cell to the Australian Economy Contents, 2015. Retrieved from https://www.newcastle.edu.au/_data/assets/pdf_file/0005/187610/Value-of-the-Jameson-Cell-to-the-Australian-Economy-1990-2014-with-cover.pdf.
[8] C.D.F. Gontijo, D. Fornasiero, J. Ralston, The limits of fine and coarse particle flotation, Can. J. Chem. Eng. 85 (6) (2008) 739–747, https://doi.org/10.1002/cjce.5450850519.
[9] P.B. Kowalczuk, O. Sahbaz, J. Drzymala, Maximum size of floating particles in different flotation cells, Miner. Eng. 24 (8) (2011) 766–771, https://doi.org/10.1016/j.mineng.2011.01.007.
[10] C.M. Phan, A.V. Nguyen, J.D. Miller, G.M. Evans, G.J. Jameson, Investigations of bubble-particle interactions, Int. J. Miner. Process. 72 (1-4) (2003) 239–254.
[11] L. Ge, G.M. Evans, R. Moreno-Atanasio, CFD-DEM investigation of the interaction between a particle swarm and a stationary bubble: Particle-bubble collision efficiency, Powder Technol. 366 (2020) 641–652.
[12] G. Wang, A.V. Nguyen, S. Mitra, J.B. Joshi, G.J. Jameson, G.M. Evans, A review of the mechanisms and models of bubble-particle detachment in froth flotation, Sep. Purif. Technol. 170 (2016) 155–172, https://doi.org/10.1016/j.seppur.2016.06.041.
[13] B. Bai, N.P. Hankins, M.J. Hey, S.W. Kingman, In situ mechanistic study of SDS adsorption on hematite for optimized froth flotation, Ind. Eng. Chem. Res. 43 (18) (2004) 5326–5338, https://doi.org/10.1021/ie034307t.
[14] A.A. Mohammed, S.E. Ebrahim, A.I. Alwared, Flotation and sorptive-flotation methods for removal of lead ions from wastewater using SDS as surfactant and barley husk as biosorbent, J. Chem., 2013, 413948. 10.1155/2013/413948.
[15] X. Zeng, X. Longhua, J. Tian, Y. Wanzhong, Y. Yang, W. Deng, Effect of a CA depressant on flotation separation of celestite from fluorite and calcite using SDS as a collector, Miner. Eng. 111 (2017) 201–208, https://doi.org/10.1016/j.mineng.2017.06.019.
[16] K. Sun, T. Liu, Y. Zhang, X. Liu, B. Wang, C. Xu, Application and Mechanism of Anionic Collector Sodium Dodecyl Sulfate (SDS) in Phosphate Beneficiation, Minerals 7 (2) (2017) 29, https://doi.org/10.3390/min7020029.
[17] W.S. Ng, L.A. Connal, E. Forbes, G.V. Franks, A review of temperature-responsive polymers as novel reagents for solid-liquid separation and froth flotation of minerals, Miner. Eng. 123 (2018) 144–159, https://doi.org/10.1016/j.mineng.2018.03.027.
[18] W.S. Ng, L.A. Connal, E. Forbes, K. Mohanarangam, G.V. Franks, *In situ* study of aggregate sizes formed in chalcopyrite-quartz mixture using temperature-responsive polymers, Adv. Powder Technol. 29 (8) (2018) 1940–1949, https://doi.org/10.1016/j.apt.2018.04.027.
[19] B.P. Binks, Particles as surfactants - Similarities and differences, Curr. Opin. Colloid Interface Sci. 7 (4–5) (2002) 21–41, https://doi.org/10.1016/S1359-0294(02)00008-0.
[20] S. Stiller, H. Gers-Barlag, M. Lergenmueler, F. Pflucker, J. Schulz, K.P. Wittern, R. Daniels, Investigation of the stability in emulsions stabilized with different surface modified titanium dioxides, Colloids Surf. A Physicochem. Eng. Asp. 232 (1–2) (2004) 261–267, https://doi.org/10.1016/j.colsurfa.2003.11.003.

[21] S. Simovic, C.A. Prestidge, Hydrophilic silica nanoparticles at the PDMS droplet-water interface, Langmuir 19 (10) (2003) 3785–3792, https://doi.org/10.1021/la026803c.

[22] S. Abend, N. Bonnke, U. Gutschner, G. Lagaly, Stabilization of emulsions by heterocoagulation of clay minerals and layered double hydroxides, Colloid Polym. Sci. 276 (8) (1998) 730–737, https://doi.org/10.1007/s003960050303.

[23] R.J. Pugh, Bubble and foam chemistry. Cambridge University Press, 2016.

[24] T.N. Hunter, E.J. Wanless, G.J. Jameson, Effect of esterically bonded agents on the monolayer structure and foamability of nano-silica, Colloids Surf A Physicochem Eng Asp 334 (1–3) (2009) 181–190, https://doi.org/10.1016/j.colsurfa.2008.10.039.

[25] A.P.G. Lockwood, J.R.L. Rumney, M.G. Barnes, M. Dodds, J. Peakall, T.N. Hunter, (Approximation of hindered zonal settling rates for flocculated inorganic/organic composite suspensions in inertial flow conditions. Journal of Water Process Engineering, 51, 103459, 2023. 10.1016/j.jwpe.2022.103459.

[26] A.P.G. Lockwood, J. Peakall, N.J. Warren, G. Randall, M. Barnes, D. Harbottle, T. N. Hunter, Structure and sedimentation characterisation of sheared $Mg(OH)_2$ suspensions flocculated with anionic polymers, Chem. Eng. Sci. 231 (2021), 116274, https://doi.org/10.1016/j.ces.2020.116274.

[27] L.F. Mortimer, M. Fairweather, Prediction of polymer extension, drag reduction, and vortex interaction in direct numerical simulation of turbulent channel flows, Phys. Fluids 34 (7) (2022), https://doi.org/10.1063/5.0094978.

[28] C.F. Lu, L.A. Spielmant, Kinetics of floc breakage and aggregation in agitated liquid suspensions, Colloid Interface Sci. 103 (1985) 95–105, https://doi.org/10.1016/0021-9797(85)90080-3.

[29] Y. Kyoda, A.D. Costine, P.D. Fawell, J. Bellwood, G.K. Das, Using focused beam reflectance measurement (FBRM) to monitor aggregate structures formed in flocculated clay suspensions, Miner. Eng. 138 (2019) 148–160, https://doi.org/10.1016/j.mineng.2019.04.045.

[30] S. Sun, M. Weber-Shirk, L.W. Lion, Characterization of Flocs and Floc Size Distributions Using Image Analysis, Environ. Eng. Sci. 33 (2016) 25–34, https://doi.org/10.1089/ees.2015.0311.

[31] L. Guérin, C. Frances, A. Liné, C. Coufort-Saudejaud, Fractal dimensions and morphological characteristics of aggregates formed in different physico-chemical and mechanical flocculation environments, Colloids Surfaces A Physicochem. Eng. Asp. 560 (2019) 213–222, https://doi.org/10.1016/j.colsurfa.2018.10.017.

[32] Z. Yang, H. Yang, Z. Jiang, X. Huang, L. Haibo, A. Li, R. Cheng, A new method for calculation of flocculation kinetics combining Smoluchowski model with fractal theory, Colloids Surfaces A Physicochem. Eng. Asp. 423 (2013) 11–19, https://doi.org/10.1016/j.colsurfa.2013.01.058.

[33] P. Jarvis, B. Jefferson, S.A. Parsons, Floc structural characteristics using conventional coagulation for a high doc, low alkalinity surface water source, Water Res. 40 (2006) 2727–2737, https://doi.org/10.1016/j.watres.2006.04.024.

[34] M.S. Nasser, A.E. James, The effect of polyacrylamide charge density and molecular weight on the flocculation and sedimentation behaviour of kaolinite suspensions, Sep. Purif. Technol. 52 (2006) 241–252, https://doi.org/10.1016/j.seppur.2006.04.005.

[35] M.S. Nasser, A.E. James, The effect of electrolyte concentration and pH on the flocculation and rheological behaviour of kaolinite suspensions, J. Eng. Sci. Technol. 4 (2009) 430–446.

[36] G.V. Franks, P.D. Yates, N.W.A. Lambert, G.J. Jameson, Aggregate size and density after shearing, implications for dewatering fine tailings with hydrocyclones, Int. J. Miner. Process. 77 (2005) 46–52, https://doi.org/10.1016/j.minpro.2005.02.002.

[37] Y. Zhou, G.V. Franks, Flocculation Mechanism Induced by Cationic Polymers Investigated by Light Scattering, Langmuir 22 (2006) 6775–6786, https://doi.org/10.1021/la060281+.

[38] W.S. Ng, R. Sonsie, E. Forbes, Flocculation/flotation of hematite fines with anionic temperature-responsive polymer acting as a selective flocculant and collector, Minerals Enigneering 77 (2015) 64–71.

[39] E. Carissimi, J. Rubio, Polymer-bridging flocculation performance using turbulent pipe flow, Miner. Eng. 70 (2015) 20–25, https://doi.org/10.1016/j.mineng.2014.08.019.

[40] A.B. Said, F. Frances, A. Grandjean, C. Larille, S. Faure, Study of a foam flotation process assisted by cationic surfactant for the separation of soil clay particles: processing parameters and scaling-up sensitivity, Chemical Enigneering and Processing- Process Intensification 142 (2019) 107547.

[41] W.S. Ng, L. Cooper, L.A. Connal, E. Forbes, G.J. Jameson, G.V. Franks, Tuneable collector/depressant behaviour of xanthate-functional temperature-responsive polymers in the flotation of copper sulfide: Effect of shear and temperature, Miner. Eng. 117 (2018) 91–99, https://doi.org/10.1016/j.mineng.2017.12.008.

[42] S. Sakohara, K. Nishikawa, Compaction of TiO_2 suspension utilizing hydrophilic/hydrophobic transition of cationic thermosensitive polymers, J. Colloid Interface Sci. 278 (2) (2004) 304–309, https://doi.org/10.1016/j.jcis.2004.06.002.

[43] S. Sakohara, T. Kawachi, T. Gotoh, T. Iizawa, Consolidation of suspended particles by using dual ionic thermosensitive polymers with incorporated a hydrophobic component, Sep. Purif. Technol. 106 (2013) 90–96, https://doi.org/10.1016/j.seppur.2012.12.030.

[44] W.S. Ng, L.A. Connal, E. Forbes, K. Mohanarangam, G.V. Franks, *In situ* investigation of aggregate sizes formed using thermo-responsive polymers: Effect of temperature and shear, J. Colloid Interface Sci. 494 (2017) 139–152, https://doi.org/10.1016/j.jcis.2017.01.067.

[45] J.P. O'Shea, G.G. Qiao, G.V. Franks, Temperature-responsive solid-liquid separations with charged block-copolymers of poly(N-isopropyl acryamide), Langmuir 28 (2) (2012) 905–913, https://doi.org/10.1021/la2038872.

[46] H. Li, J.P. O'Shea, G.V. Franks, Effect of molecular weight of poly(N-isopropyl acrylamide) temperature-sensitive flocculants on dewatering, AIChE J 55 (8) (2009) 2070–2080, https://doi.org/10.1002/aic.11859.

[47] S. Sakohara, R. Hinago, H. Ueda, Compaction of TiO_2 suspension by using dual ionic thermosensitive polymers, Sep. Purif. Technol. 63 (2) (2008) 319–323, https://doi.org/10.1016/j.seppur.2008.05.014.

[48] L. Wang, Y. Liu, Y. Liu, Y. Mao, J. Han, W. Li, Y. Wang, Recyclable aptamer-derived aqueous two-phase flotation for high-efficiency separation of mercury(II) ions modulated by aggregation states, Sep. Purif. Technol. 274 (2021), https://doi.org/10.1016/j.seppur.2021.118917.

[49] Z. Wang, N. Liu, D. Zou, Interface adsorption mechanism of the improved flotation of fine pyrite by hydrophobic flocculation, Sep. Purif. Technol. 275 (2021), 119245, https://doi.org/10.1016/j.seppur.2021.119245.

[50] A. Blanazs, S.P. Armes, A.J. Ryan, Self-assembled block copolymer aggregates: from micelles to vesicles and their biological applications, Macro-molecular Rapid Commun. 30 (4–5) (2009) 267–277, https://doi.org/10.1002/marc.200800713.

[51] Y. Mai, A. Eisenberg, Self-assembly of block copolymers, Chem. Soc. Rev. 41 (18) (2012) 5969–5985, https://doi.org/10.1039/C2CS35115C.

[52] K. Kataoka, Y. Nagasaki, H. Otsuka, Self-assembly of block copolymers, Mater. Today 4 (6) (2001) 30–36, https://doi.org/10.1016/S1369-7021(01)80036-5.

[53] L.Y. Liu, G. Xia, Z.J. Feng, Q.H. Hao, H.G. Tan, Self-assembly of polyelectrolyte diblock copolymers at monovalent and multivalent counterions, Soft Matter 15 (18) (2019) 3689–3699, https://doi.org/10.1039/C9SM00028C.

[54] J.R. Lovett, N.J. Warren, S.P. Armes, M.J. Smallridge, R.B. Cracknell, Order-Order Morphological Transitions for Dual Stimulus Responsive Diblock Copolymer Vesicles, Macromolecules 49 (4) (2016) 1016–1025, https://doi.org/10.1021/acs.macromol.5b02470.

[55] K. Sakai, E.G. Smith, G.B. Webber, M. Baker, E.J. Wanless, V. Butun, S.P. Armes, S. Biggs, pH-responsive behavior of selectively quaternized diblock copolymers adsorbed at the silica/aqueous solution interface, J. Colloid Interface Sci. 314 (1) (2007) 381–388, https://doi.org/10.1016/j.jcis.2007.06.018.

[56] K. Sakai, E.G. Smith, G.B. Webber, E.J. Wanless, V. Butun, S.P. Armes, S. Biggs, Effects of copolymer concentration and chain length on the pH-responsive behavior of diblock copolymer micellar films, J. Colloid Interface Sci. 303 (1) (2006) 372–379, https://doi.org/10.1016/j.jcis.2006.07.077.

[57] A.P.G. Lockwood, P.K. Shun, J. Peakall, N.J. Warren, T. Barber, N. Basharat, G. Randall, M. Barnes, D. Harbottle, T.N. Hunter, Flotation using sodium dodecyl sulphate and sodium lauroyl isethionate for rapid dewatering of $Mg(OH)_2$ radwaste suspensions, RSC Adv. 11 (30) (2021) 18661–18675.

[58] P. Kaewsaiha, K. Matsumoto, H. Matsuoka, Non-surface activity and micellization of ionic amphiphilic diblock copolymers in water. Hydrophobic chain length dependence and salt effect on surface activity and the critical micelle concentration, Langmuir 21 (22) (2005) 9938–9945, https://doi.org/10.1021/la051584r.

[59] S. Garnier, A. Laschewsky, New amphiphilic diblock copolymers: Surfactant properties and solubilization in their micelles, Langmuir 22 (10) (2006) 4044–4053, https://doi.org/10.1021/la0600595.

[60] C. Kim, S.C. Lee, J.H. Shin, J. Yoon, I.C. Kwon, S.Y. Jeong, Amphiphilic diblock copolymers based on poly(2-ethyl-2-oxazoline) and poly(1,3-trimethylene carbonate): Synthesis and micellar characteristics, Macromolecules 33 (20) (2000) 7448–7452, https://doi.org/10.1021/ma000517v.

[61] A. Ghosh, S.I. Yusa, H. Matsuoka, Y. Saruwatari, Non-surface activity and micellization behavior of cationic amphiphilic block copolymer synthesized by reversible addition-fragmentation chain transfer process, Langmuir 27 (15) (2011) 9237–9244, https://doi.org/10.1021/la201550a.

[62] A. Ghosh, S.I. Yusa, H. Matsuoka, Y. Saruwatari, Chain length dependence of non-surface activity and micellization behavior of cationic amphiphilic diblock copolymers, Langmuir 30 (12) (2014) 3319–3328, https://doi.org/10.1021/la403042p.

[63] E. Volpert, J. Selb, F. Candau, N. Green, J.F. Argillier, A. Auibert, Adsorption of hydrophobically associating polyacrylamides on clay, Langmuir 14 (8) (1998) 1870–1879, https://doi.org/10.1021/la970358h.

[64] A.R. Heath, P.A. Bahri, P.D. Fawell, J.B. Farrow, Polymer Flocculation of Calcite: Relating the Aggregate Size to the Settling Rate, AIChE J 52 (6) (2006) 1987–1994, https://doi.org/10.1002/aic.10789.

[65] F.A. Benn, P.D. Fawell, J. Halewood, P.J. Austin, A.D. Costine, W.G. Jones, N. S. Francis, D.C. Druett, D. Lester, Sedimentation and consolidation of different density aggregates formed by polymer-bridging flocculation, Chem. Eng. Sci. 184 (2018) 111–125.

[66] M. Chenal, L. Boutellier, J. Riegger, Ab *initio* RAFT emulsion polymerization of butyl arylate mediated by poly(acrylic acid) trithiocarbonate, Polym. Chem. 4 (3) (2013) 752–762, https://doi.org/10.1039/C2PY20595E.

[67] T.N. Hunter, R.J. Pugh, G.V. Franks, G.J. Jameson, The role of particles in stabilising foams and emulsions, Adv. Colloid Interface Sci. 137 (2008) 57–81, https://doi.org/10.1016/j.cis.2007.07.007.

[68] K. Hadler, M. Greyling, N. Plint, J.J. Cilliers, The effect of froth depth on air recovery and flotation performance, Miner. Eng. 36–38 (2012) 248–253, https://doi.org/10.1016/j.mineng.2012.04.003.

[69] F. Melo, J.S. Laskowski, Fundamental properties of flotation frothers and their effect on flotation, Miner. Eng. 19 (7) (2006) 766–773, https://doi.org/10.1016/j.mineng.2005.09.031.

[70] K.R. Hallam, P.C. Minshall, P.J. Heard, P.E.J. Flewitt, Corrosion of the alloys Magnox AL80, Magnox ZR55 and pure magnesium in air containing water vapour, Corros. Sci. 112 (2016) 347–363.

[71] M. Johnson, J. Peakall, M. Fairweather, S. Biggs, D. Harbottle, T.N. Hunter, Characterization of Multiple Hindered Settling Regimes in Aggregated Mineral Suspensions, Ind. Eng. Chem. Res. 55 (37) (2016) 9983–9993, https://doi.org/10.1021/acs.iecr.6b02383.

[72] Z. Maher, P. Ivanov, L. O'Brien, H. Sims, R.J. Taylor, S.L. Heath, F.R. Livens, D. Goddard, S. Kellet, P. Rand, N.D. Bryan, Americium and plutonium association with magnesium hydroxide colloids in alkaline nuclear industry process environments, J. Nucl. Mater. 468 (2016) 84–96, https://doi.org/10.1016/j.jnucmat.2015.11.010.

[73] S. Perrier, 50th Anniversary Perspective: RAFT Polymerization - A User Guide, Macromolecules 50 (19) (2017) 7433–7447, https://doi.org/10.1021/acs.macromol.7b00767.

[74] O. Colombani, M. Ruppel, F. Schubert, H. Zettl, D.V. Pergushov, A.H.E. Muller, Synthesis of Poly(n-butyl acrylate)-block-poly(acrylic acid) Diblock Copolymers by ATRP and Their Micellization in Water, Macromolecules 40 (13) (2007) 4338–4350, https://doi.org/10.1021/ma0609578.

[75] M.I. Jeraal, K.J. Roberts, I. McRobbie, D. Harbottle, Process-Focused Synthesis, Crystallization, and Physicochemical Characterization of Sodium Lauroyl Isethionate, ACS Sustain. Chem. Eng. 6 (3) (2018) 2667–2675, https://doi.org/10.1021/acssuschemeng.7b04237.

[76] Y.D. Yan, S.M. Glover, G.J. Jameson, S. Biggs, The flocculation efficiency of polydisperse polymer flocculants, Int. J. Miner. Process. 73 (2–4) (2004) 161–175, https://doi.org/10.1016/S0301-7516(03)00071-1.

[77] J.D. Berry, M.J. Neeson, R.R. Dagastine, D.Y.C. Chan, R.F. Tabor, Measurement of surface and interfacial tension using pendant drop tensiometry, J. Colloid Interface Sci. 454 (2015) 226–237, https://doi.org/10.1016/j.jcis.2015.05.012.

[78] A.J. Morse, E.C. Giakoumatos, S. Tan, G.B. Webber, S.P. Armes, S. Ata, E. J. Wanless, Giant pH-responsive microgel colloidosomes: Preparation, interaction dynamics and stability, Soft Matter 12 (7) (2016) 1477–1486, https://doi.org/10.1039/C5SM02450A.

[79] A.J. Morse, S. Tan, E.C. Giakoumatos, G.B. Webber, S.P. Armes, S. Ata, E. J. Wanless, Arrested coalescence behaviour of giant Pickering droplets and colloidosomes stabilised by poly(tert-butylaminoethyl methacrylate) latexes, Soft Matter 10 (36) (2014) 5669–5681, https://doi.org/10.1039/C4SM00801D.

[80] K.L. Thompson, E.C. Giakoumatos, S. Ata, G.B. Webber, S.P. Armes, E.J. Wanless, Direct observation of giant pickering emulsion and colloidosome droplet interaction and stability, Langmuir 28 (44) (2012) 16501–16511, https://doi.org/10.1021/la3025765.

[81] R. Shanti, A.N. Hadi, Y.S. Salim, S.Y. Chee, S. Ramesh, K. Ramesh, Degradation of ultra-high molecular weight poly(methyl methacrylate-co-butyl acrylate-co-acrylic acid) under ultra violet irradiation, RSC Adv. 7 (2) (2017) 112–120, https://doi.org/10.1039/C6RA25313J.

[82] C.M. Sorensen, Light Scattering by Fractal Aggregates: A Review, Aerosol Sci. Tech. 35 (2) (2001) 648–687.

[83] F. Hernáinz, A. Caro, Variation of surface tension in aqueous solutions of sodium dodecyl sulfate in the flotation bath, Colloids Surf A Physicochem Eng Asp 196 (2002) 19–24, https://doi.org/10.1016/S0927-7757(01)00575-1.

[84] H. Zettl, Y. Portnoy, M. Gottlieb, G. Krausch, Investigation of Micelle Formation by Fluorescence Correlation Spectroscopy, J. Phys. Chem. B 109 (27) (2005) 13397–13401.

[85] H. Matsuoka, S. Maeda, P. Kaewsaiha, K. Matsumoto, Micellization of non-surface-active diblock copolymers in water. Special characteristics of poly (styrene)-block-poly(styrenesulfonate), Langmuir 20 (17) (2004) 7412–7421, https://doi.org/10.1021/la0492153.

[86] H. Matsuoka, M. Matsutani, E. Mouri, K. Matsumoto, Polymer micelle formation without Gibbs monolayer formation: Synthesis and characteristic behavior of an amphiphilic diblock copolymer having strong acid groups, Macromolecules 36 (14) (2003) 5321–5330, https://doi.org/10.1021/ma0215161.

[87] P. Guenoun, H.T. Davis, M. Tirrell, J.W. Mays, Aqueous micellar solutions of hydrophobically modified polyelectrolytes, Macromolecules 29 (11) (1996) 3965–3969, https://doi.org/10.1021/ma946438z.

[88] M. Jacquin, P. Muller, R. Talingting-Pabalan, H. Cottet, J.F. Berret, T. Futterer, O. Theodoly, Chemical analysis and aqueous solution properties of charged amphiphilic block copolymers PBA-b-PAA synthesized by MADIX®, J. Colloid Interface Sci. 316 (2) (2007) 897–911, https://doi.org/10.1016/j.jcis.2007.08.025.

[89] J. Wittmer, J.F. Joanny, Charged Diblock Copolymers at Interfaces, Macromolecules 26 (11) (1993) 2691–2697, https://doi.org/10.1021/ma00063a009.

[90] E. Eghbali, O. Colombani, M. Drechsler, A.H.E. Müller, H. Hoffmann, Rheology and phase behavior of poly(n-butyl acrylate)-block-poly(acrylic acid) in aqueous solution, Langmuir 22 (11) (2006) 4766–4776, https://doi.org/10.1021/la053272u.

[91] L.A. Trujillo-Cayado, P. Ramírez, L.M. Pérez-Mosqueda, M.C. Alfaro, J. Muñoz, Surface and foaming properties of polyoxyethylene glycerol ester surfactants, Colloids Surf A Physicochem Eng Asp 458 (2014) 195–202, https://doi.org/10.1016/j.colsurfa.2014.02.009.

[92] P.A. Yazhgur, A.V. Akent'ev, A.Y. Bilibin, I.M. Zorin, B.A. Noskov, Dynamic surface properties of sodium N-acryloyl-11-amimoundecanoate and poly(sodium N-acryloyl-11-aminoundecanoate), Colloid J. 74 (6) (2012) 743–750.

[93] P. Degen, M. Paulus, E. Zwar, V. Jakobi, S. Dogan, M. Tolan, H. Rehage, Surfactant-mediated formation of alginate layers at the water-air interface, Surf. Interface Anal. 51 (11) (2019) 1051–1058.

[94] F. Monroy, J. Giermanska Kahn, D. Langevin, Dilational viscoelasticity of surfactant monolayers, Colloids Surf. A Physicochem. Eng. Asp. 143 (1) (1998) 251–260, https://doi.org/10.1016/S0927-7757(98)00373-2.

[95] Q. Zhang, Q. Zhang, Y. Li, L. Cao, L. Li, K. Huang, W. Li, C. Yang, Dilational Viscoelastic Properties of Water-Fuel Interfaces in Single and Binary Surfactant Systems, Energy Fuel 33 (11) (2019) 9055–9066, https://doi.org/10.1021/acs.energyfuels.9b00517.

[96] T. Moon, R. Nagarajan, Deinking xerographic and laser-printed paper using block copolymers, Colloids Surf. A Physicochem. Eng. Asp. 132 (2–3) (1998) 275–288, https://doi.org/10.1016/S0927-7757(97)00175-1.

[97] P. Ofori, G. O'Brien, B. Firth, C. McNally, The Use of Tri-Block Copolymer Surfactants as Promoters to Improve Flotation Recovery of Poorly Floating Coal Components, Int. J. Coal Prep. Util. 32 (2) (2012) 103–119, https://doi.org/10.1080/19392699.2011.640298.

[98] B.A. Noskov, S.Y. Lin, G. Loglio, R.G. Rubio, R. Miller, Dilational viscoelasticity of PEO-PPO-PEO triblock copolymer films at the air-water interface in the range of high surface pressures, Langmuir 22 (6) (2006) 2647–2652, https://doi.org/10.1021/la052662d.

[99] M.S. Manga, T.N. Hunter, O.J. Cayre, D.W. York, M.D. Reichert, S.L. Anna, L. M. Walker, R.A. Williams, S.R. Biggs, Measurements of Submicron Particle Adsorption and Particle Film Elasticity at Oil-Water Interfaces, Langmuir 32 (17) (2016) 4125–4133, https://doi.org/10.1021/acs.langmuir.5b04586.

[100] J. Gregory, S. Barany, Adsorption and flocculation by polymers and polymer mixtures, Adv. Colloid Interface Sci. 169 (1) (2011) 1–12, https://doi.org/10.1016/j.cis.2011.06.004.

[101] H.J. Ploehn, Self-consistent field theory for polymer adsorption: Molecular volume effects, Colloids Surf A Physicochem Eng Asp 86 (1994) 25–40, https://doi.org/10.1016/0927-7757(93)02687-A.

[102] J.M.H.M. Scheutjens, G.J. Fleer, Statistical theory of the adsorption of interacting chain molecules. 1. Partition function, segment density distribution, and adsorption isotherms, J. Phys. Chem. 83 (12) (1979) 1619–1635, https://doi.org/10.1021/j100475a012.

[103] T. Swift, L. Swanson, M. Geoghegan, S. Rimmer, The pH-responsive behaviour of poly(acrylic acid) in aqueous solution is dependent on molar mass, Soft Matter 12 (9) (2016) 2542–2549.

[104] J.L. Lin, C. Huang, C.J.M. Chin, J.R. Pan, Coagulation dynamics of fractal flocs induced by enmeshment and electrostatic patch mechanisms, Water Res. 42 (17) (2008) 4457–4466, https://doi.org/10.1016/j.watres.2008.07.043.

[105] G.C. Bushell, Y.D. Yan, D. Woodfield, J. Raper, R. Amal, On techniques for the measurement of the mass fractal dimension of aggregates, Adv. Colloid Interface Sci. 95 (2002) 1–50, https://doi.org/10.1016/S0001-8686(00)00078-6.

[106] L. de Martín, A. Fabre, J. Ruud van Ommen, The fractal scaling of fluidized nanoparticle agglomerates, Chem. Eng. Sci. 112 (2014) 79–86, https://doi.org/10.1016/j.ces.2014.03.024.

[107] J. Lasue, I. Maroger, R. Botet, P.H. Garnier, S. Merouane, T.H. Mannel, A. C. Levasseur-Regourd, M.S. Bentley, Flattened loose particles from numerical simulations compared to particles collected by Rosetta, A & A 630 (2019) A28, https://doi.org/10.1051/0004-6361/201834766.

[108] S.K. Friedlander, Smoke, dust, and haze: Fundamentals of aerosol dynamics, Oxford University Press, 2000.

[109] F. Xiao, K.M. Lam, X. Li, Investigation and visualization of internal flow through particle aggregates and microbial flocs using particle image velocimetry, J. Colloid Interface Sci. 397 (2013) 163–168, https://doi.org/10.1016/j.jcis.2013.01.053.

[110] N. Paul, S. Biggs, J. Shiels, R.B. Hammond, M. Edmondson, L. Maxwell, D. Harbottle, T.N. Hunter, Influence of shape and surface charge on the sedimentation of spheroidal, cubic and rectangular cuboid particles, Powder Technol. 322 (2017) 75–83, https://doi.org/10.1016/j.powtec.2017.09.002.

[111] B. Shi, Q. Wei, D. Wang, Z. Zhu, H. Tang, Coagulation of humic acid: The performance of preformed and non-preformed Al species, Colloids Surf A Physicochem Eng Asp 296 (1–3) (2007) 141–148, https://doi.org/10.1016/j.colsurfa.2006.09.037.

[112] D. Ghernaout, B. Ghernaout, Sweep flocculation as a second form of charge neutralisation—a review, Desalin. Water Treat. 44 (1–3) (2012) 15–28, https://doi.org/10.1080/19443994.2012.691699.

[113] E. Forbes, D. Bradshaw, G.V. Franks, Temperature sensitive polymers as efficient and selective flotation collectors, Miner. Eng. 24 (8) (2011) 772–777, https://doi.org/10.1016/j.mineng.2011.02.003.

[114] A. Norori-McCormac, P.R. Brito-Parada, K. Hadler, K. Cole, J.J. Cilliers, The effect of particle size distribution on froth stability in flotation, Sep. Purif. Technol. 184 (2017) 240–247, https://doi.org/10.1016/j.seppur.2017.04.022.

[115] H.B. Ortiz-Oliveros, R.M. Flores-Espinosa, Design of a mobile dissolved air flotation system with high rate for the treatment of liquid radioactive waste, Process Saf. Environ. Prot. 144 (2020) 23–31, https://doi.org/10.1016/j.psep.2020.07.016.